iScience

CellPress
OPEN ACCESS

Article

GIV/Girdin and Exo70 Collaboratively Regulate the Mammalian Polarized Exocytic Machinery

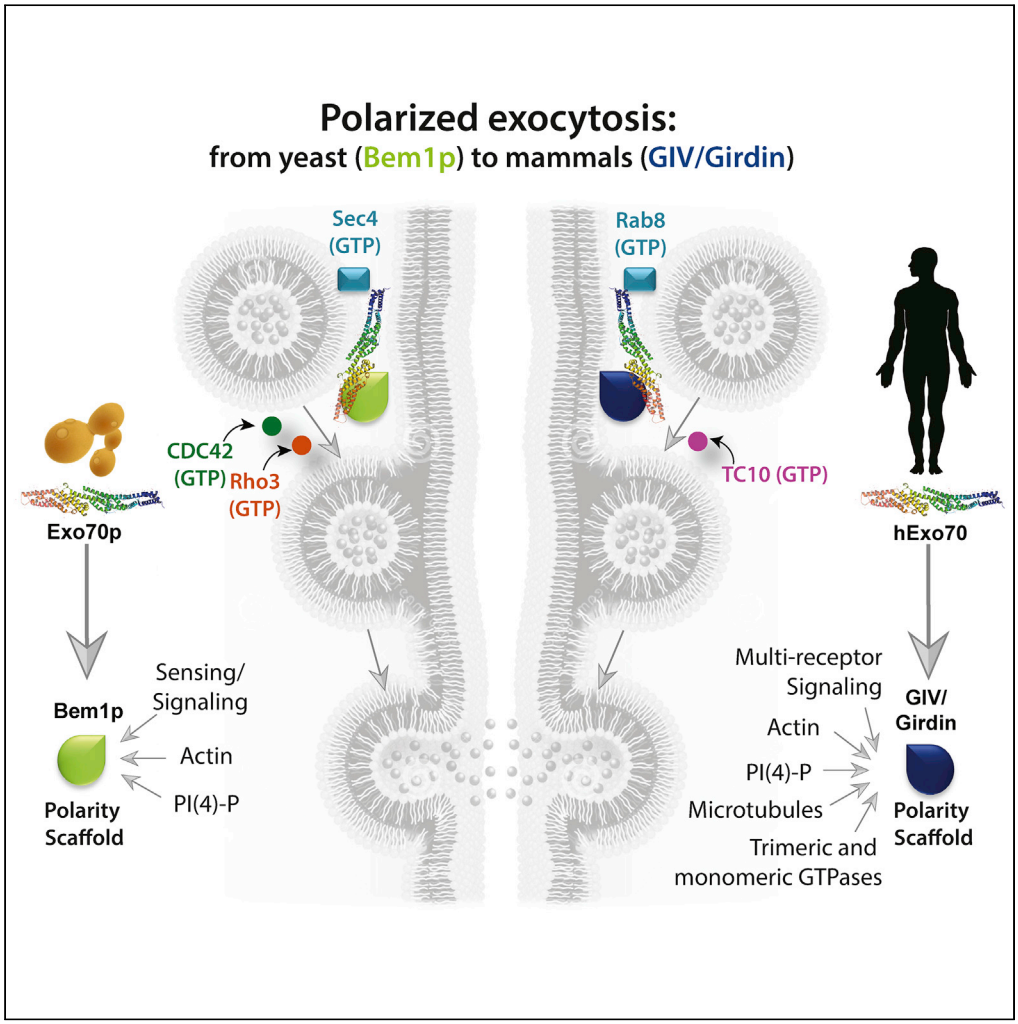

Cristina Rohena, Navin Rajapakse, I-Chung Lo, Peter Novick, Debashis Sahoo, Pradipta Ghosh

prghosh@ucsd.edu

HIGHLIGHTS

GIV (human) and Bem1p (yeast) bind Exo70 and are required for exocytosis•

GIV binds and aids PM localization of Exo70 via a conserved short linear motif•

Binding facilitates MT1-MMP delivery to invadosomes, ECM degradation, and invasion•

Regulatory control over polarized exocytosis is enriched during evolution

Rohena et al., iScience 23, 101246
July 24, 2020
https://doi.org/10.1016/j.isci.2020.101246

iScience

CellPress
OPEN ACCESS

Article

GIV/Girdin and Exo70 Collaboratively Regulate the Mammalian Polarized Exocytic Machinery

Cristina Rohena,[1] Navin Rajapakse,[2] I-Chung Lo,[2] Peter Novick,[2] Debashis Sahoo,[3,4,5] and Pradipta Ghosh[1,2,5,6,7,*]

SUMMARY

Polarized exocytosis is a fundamental process by which membranes and cargo proteins are delivered to the cell surface with precise spatial control. Although the need for the octameric exocyst complex is conserved from yeast to humans, what imparts spatial control is known only in yeast, i.e., a polarity scaffold called Bem1p. We demonstrate here that the mammalian scaffold protein, GIV/Girdin, fulfills the key criteria and functions of its yeast counterpart Bem1p; both bind Exo70 proteins via similar short-linear interaction motifs, and each prefers its evolutionary counterpart. Selective disruption of the GIV·Exo-70 interaction derails the delivery of the metalloprotease MT1-MMP to invadosomes and impairs collagen degradation and haptotaxis through basement membrane matrix. GIV's interacting partners reveal other components of polarized exocytosis in mammals. Findings expose how the exocytic functions aid GIV's pro-metastatic functions and how signal integration via GIV may represent an evolutionary advancement of the exocytic process in mammals.

INTRODUCTION

Exocytosis is an essential process in all eukaryotic cells, defined as the delivery of intracellular contents such as hormones, mRNAs, and proteins between secretory vesicles and the plasma membrane (PM). The spatially controlled fusion of these secretory vesicles with the PM requires SNARE proteins. However, before vesicle fusion with the PM, vesicles must first be anchored to the membrane by the octameric exocyst complex. First identified in *S. cerevisiae*, using a variety of biochemical and genetic approaches (Terbush et al., 1996; Terbush and Novick, 1995; Novick et al., 1980), the exocyst complex is an evolutionarily conserved macromolecular complex composed of Sec3, Sec5, Sec6, Sec8, Sec10, Sec15, Exo70, and Exo84. Evidence suggests that it is this exocyst complex that imparts spatial and temporal control of exocytosis and that such precision control is critical for a myriad of cellular processes, such as morphogenesis, cell cycle progression, primary ciliogenesis, cell migration, and tumor invasion (Wu and Guo, 2015).

When it comes to spatial control, it appears that the process of exocytosis is highly polarized. Yeast genetics, and biochemical (Boyd et al., 2004) and structural studies using cryoelectron microscope and 3D molecular modeling (Mei et al., 2018) in yeast have suggested that the exocyst complex is assembled in a hierarchical manner and that several such complexes may cooperatively ensure the fidelity in recruiting the vesicle to the appropriate exocytic site on the PM (Picco et al., 2017). For example, in the budding yeast, the exocyst is localized to the emerging bud tip, where it mediates exocytosis for the asymmetric expansion of daughter cell surfaces during polarized cell growth. During cytokinesis, the exocyst is localized to the mother-daughter cell junction to mediate abscission (Terbush and Novick, 1995, Finger et al., 1998; Guo et al., 1999; Zhang et al., 2008). Exo70p and Sec3p were identified as the key subunits of the octameric complex, which plays a pivotal role in targeting of the exocyst to specific sites on the PM (Boyd et al., 2004). Such polarized localization of Exo70p and Sec3p cannot be attributed to t-SNARE (target-Soluble NSF-Attachment Protein Receptor) proteins, because the latter distributed along the entire PM (Brennwald et al., 1994). Who or what imparts polarity to the process of exocytosis remained unknown until systematic studies employing Exo70p mutants and yeast genetics pinpointed that a specific stretch of Exo70p (i.e., domain C) must interact with some other actin-independent polarity determinant (Hutagalung et al., 2009), which was subsequently identified as the multidomain polarity scaffold and bud emergence protein, Bem1p (Liu and Novick, 2014). This Exo70p•Bem1p interaction was implicated in polarizing the process of vesicle

[1]Department of Medicine, University of California San Diego, 9500 Gilman Drive (MC 0651), George E. Palade Bldg, Rm 232, 239, La Jolla, CA 92093, USA

[2]Department of Cellular and Molecular Medicine, University of California San Diego, San Diego, CA 92093, USA

[3]Department of Pediatrics, University of California San Diego, San Diego, CA 92093, USA

[4]Department of Computer Science and Engineering, Jacob's School of Engineering, University of California San Diego, San Diego, CA 92093, USA

[5]Rebecca and John Moore Comprehensive Cancer Center, University of California San Diego, San Diego, CA 92093, USA

[6]Veterans Affairs Medical Center, 3350 La Jolla Village Dr, San Diego, CA 92161, USA

[7]Lead Contact

*Correspondence: prghosh@ucsd.edu

https://doi.org/10.1016/j.isci.2020.101246

exocytosis in yeast; binding-deficient mutants of Exo70p were incapable of tethering secretory vesicles to cortical sites specified by Bem1p (Liu and Novick, 2014).

Although the fundamentals of exocytosis were discovered first in yeast, its existence and importance in mammals is widely accepted as a driver in multiple disease states in humans (Martin-Urdiroz et al., 2016), and insights into how the process is regulated in mammals remains unknown to date. As in yeast, the mammalian Exo70 has been the most studied subunit; these studies have revealed that although the composition of the canonical octameric exocyst component is essentially invariant (Boehm and Field, 2019), there is, however, a remarkable degree of evolutionary flexibility to allow for specialization through diversity in exocytic mechanism and building more regulatory control along the way. For example, unlike yeast Exo70p, mammalian Exo70 interacts directly with Arp2/3 complex during cell migration and enhances actin cytoskeleton remodeling (Zuo et al., 2006). Mammalian Exo70 is also under the control of growth factors—epidermal growth factor stimulation triggers phosphorylation of Exo70 by ERK1/2 leading to enhanced octameric complex formation, matrix metalloproteinase (MMP) secretion, and cell invasion (Zhao et al., 2013; He et al., 2007; Lu et al., 2013; Hertzog et al., 2012; Liu et al., 2009). In addition, a switch between Exo70 isoforms has been reported in breast cancer that correlates with a switch from epithelial to mesenchymal transition (Lu et al., 2013); the former is engaged in exocytosis, whereas the latter modulates actin dynamics. The fact that Exo70 was the only exocyst subunit found to correctly localize when overexpressed in mammalian epithelial cells (He et al., 2007; Yeaman et al., 2004) suggested that Exo70 might be the critical component that recognizes a polarity determinant at the cell cortex. In the absence of any clear mammalian counterpart of yeast polarity scaffold Bem1p, it has been speculated that other mammalian polarity determinants may fulfill that role to facilitate Exo70 recruitment in mammals. The identity of such Bem1p counterpart in humans remains unknown.

Here we reveal that the multi-modular polarity scaffold Gα-interacting vesicle-associated protein (GIV, a.k.a, Girdin) (Ohara et al., 2012; Sasaki et al., 2015; Aznar et al., 2016b) fulfills the criteria to serve as the mammalian functional homolog of the yeast polarity determinant, Bem1p. The scaffolding function of GIV has been shown to mediate the purposeful dynamic "glue"-ing of diverse signaling pathways: GIV is a guanine nucleotide exchange factor (GEF) for trimeric GTPases, Gi (Garcia-Marcos et al., 2009; Kalogriopoulos et al., 2019) and Gs (Gupta et al., 2016), a polarity scaffold that binds and modulates via G protein intermediates the aPKC/Par complexes (Sasaki et al., 2015; Ohara et al., 2012); it is a substrate of and major signaling conduit for multiple receptor and non-receptor tyrosine kinases (Lin et al., 2011; Mittal et al., 2011; Midde et al., 2018); serves as a signaling adaptor for growth factor (Lin et al., 2014), integrins (Lopez-Sanchez et al., 2015a; Leyme et al., 2015), and other classes of receptors (reviewed in Ghosh et al., 2017); and is an actin remodeler (Enomoto et al., 2005) and a scaffold for polymerized microtubules (Nechipurenko et al., 2016; Aznar et al., 2016b). Most of the work on GIV thus far has revealed its ability to serve as an integrator of multiple signaling pathways that enhances multiple fundamental cellular processes and how its dysregulation (overexpression and hyperactivation) favors cancer invasion and metastasis (reviewed in Aznar et al., 2016a). This work not only sheds light into GIV's ability to enhance a key process that aids metastasis (i.e., polarized exocytosis of matrix metalloproteases) but also reveals how the modular makeup and functional diversity of GIV imparts the process of exocytosis features of polarity and context-dependent regulation by diverse signaling pathways.

RESULTS AND DISCUSSION

GIV and Bem1p Share Key Properties, Conserved Modes of Binding to Exo70

We first began by looking for polarity scaffold proteins with the mammalian Exo70 interactome (Figure S1) using Biological General Repository for Interaction Datasets (BioGRID; thebiogrid.org). A systematic analysis of all physical interactions of Exo70 revealed that among many coiled coil multi-modular proteins, it binds the mammalian polarity scaffold GIV (encoded by the gene CCDC88A), as revealed initially in a yeast 2-hybrid screen (Camargo et al., 2007) and validated later by us as a protein that colocalizes with (as determined by confocal immunofluorescence and *in situ* proximity ligation assays) and directly binds Exo70 (Lopez-Sanchez et al., 2015b). We noted that although the modular makeup of GIV and Bem1p had very little in common (Figure 1A), GIV fulfilled some of the key functional criteria that were previously deemed as necessary for Bem1p to polarize exocytosis in yeast (Figure 1B). Furthermore, besides its ability to bind and modulate Par-polarity complexes, GIV presented numerous additional modules, functional features, and interesting interactions (Figures 1A and 1B). We hypothesized that GIV may be the long-sought evolutionary counterpart of Bem1p. Because Exo70 was proposed as the exocyst subunit that interacts with

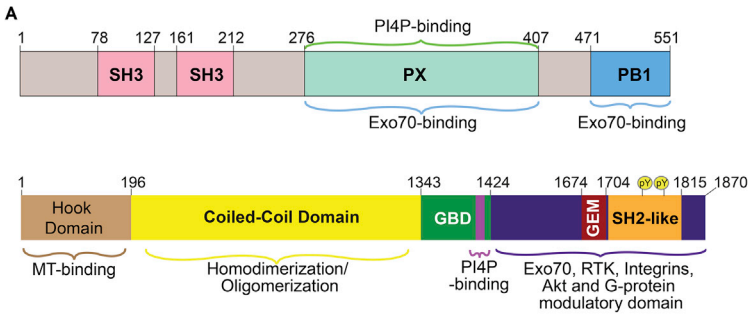

B

Protein	Species	Exo70 -binding	Polarity scaffold	PI4-P -binding	Actin-binding	Microtubules -binding
Bem1p	Yeast	✓	✓	✓	✓	χ
GIV	Mammals	✓	✓	✓	✓	✓

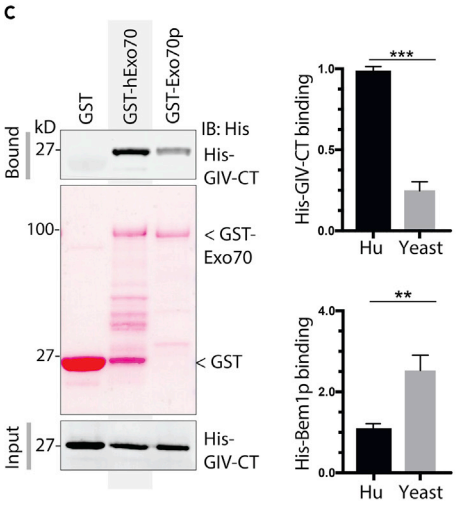

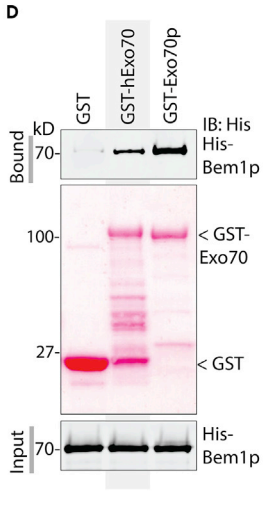

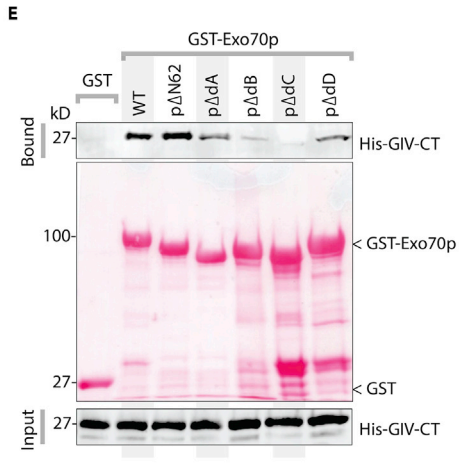

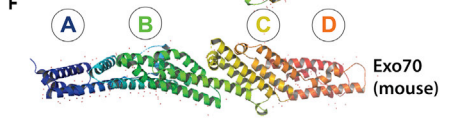

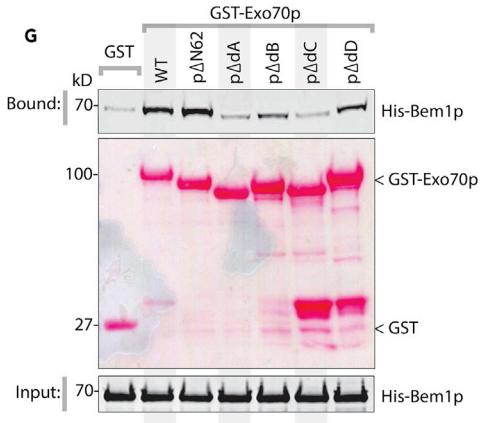

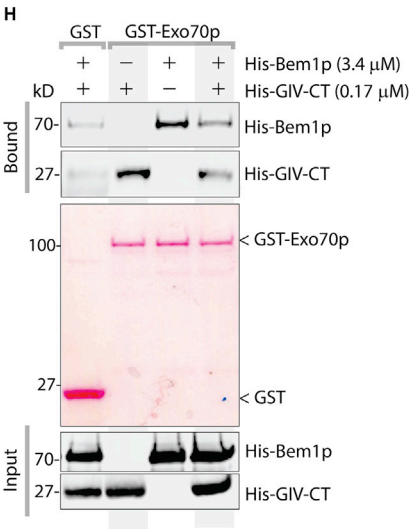

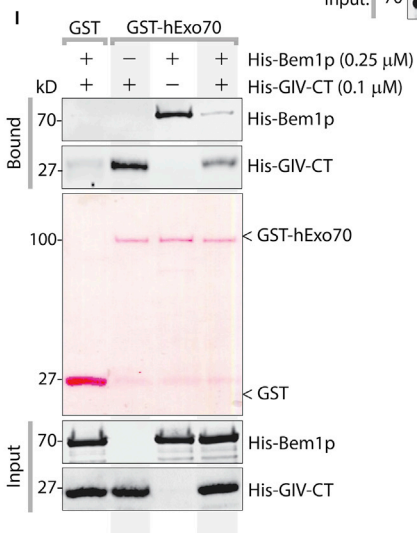

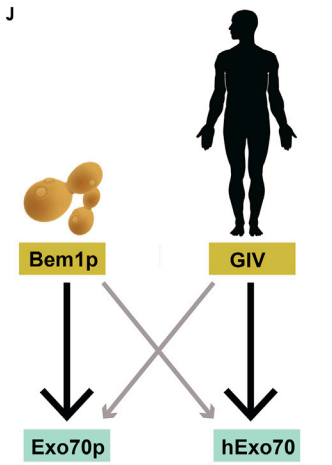

Figure 1. Polarity Scaffolds GIV and Bem1p Share Key Properties and Display Conserved Modes of Binding to Exo70

(A) Domain maps of the yeast (Bem1p [top]) and human (GIV/Girdin [bottom]) polarity scaffolds. Major interactions are annotated.

(B) Table listing key properties of Bem1p that have been implicated in its ability to impart polarity to the process of exocytosis.

(C) Recombinant His-GIV-CT (~3 μg) was used in GST pull-down assays with GST, GST-hExo70 (human), and GST-Exo70p (yeast). Bound GIV was visualized by immunoblotting using anti-His mAb. Equal loading of GST proteins was confirmed by Ponceau S staining. Top right: bar graph displays fold change in binding. Error bars represent standard error of mean; ± SEM; n = 3; ***p value = 0.001.

(D) Recombinant His-Bem1p (~3 μg) was used in GST pull-down assays with GST proteins as in (C). Bound Bem1p was visualized by immunoblotting using anti-His mAb. Equal loading of GST proteins was confirmed by Ponceau S staining. Bottom left: Bar graph displays fold change in binding. Error bars represent standard error of mean; ± SEM; n = 3; **p value = 0.01.

(E–G) Pull-down assays as in (C) were carried out using either recombinant His-GIV-CT (E) or His-Bem1p (G) and various GST constructs (Liu and Novick, 2014) lacking the indicated domains of Exo70 (yeast versus mouse comparison; (F) immobilized on glutathione beads. Bound GIV (E) or Bem1p (G) was visualized by immunoblotting using anti-His mAb. Equal loading of GST proteins was confirmed by Ponceau S staining.

(H–J) Competition between GIV and Bem1p for binding to either Exo70p (yeast; H) or hExo70 (human; I) was assessed by carrying out pull-down assays adding (+) or not (–) the soluble His-GIV-CT and His-Bem1p proteins alone or simultaneously to GST-Exo70 proteins immobilized on glutathione beads. Bound GIV or Bem1p proteins were visualized by immunoblotting using anti-His mAb. (J) Schematic summarizing the cross-species binding of Bem1p and GIV to Exo70. The size and darkness of arrows indicate binding preference.

polarity determinants in mammalian cells (He et al., 2007; Yeaman et al., 2004), we began first by comparing the abilities of Bem1p and GIV to bind yeast and human Exo70. We found that both GST-tagged human (hExo70) and yeast (Exo70p) Exo70 could bind full-length endogenous GIV (Figure S2A). Using recombinant His-tagged proteins in similar pull-down assays with GST-Exo70, we confirmed that the GIV•Exo70 interaction is direct and that the C terminus of GIV is sufficient (GIV-CT; Figure 1C). Although both Bem1p and GIV-CT could bind both yeast and human Exo70 proteins, each preferentially bound to its evolutionary counterpart (Figures 1C and 1D): GIV-CT binds four times as much to human Exo70 compared with yeast Exo70p (Figure 1C), whereas equimolar amounts of Bem1p binds two times as much to yeast Exo70p compared with human Exo70 (Figure 1D). These protein concentrations were chosen based on the published Kd of Bem1p with Exo70p (Liu and Novick, 2014); concentrations of all human proteins (GIV and Exo70) were adjusted to molar equivalents to yeast counterparts.

Prior work showed that although Bem1p forms an extended interface with Exo70p, domain C is the most critical part of Exo70 that is responsible for the interaction (Liu and Novick, 2014). Using a series of previously validated Exo70p mutants, we confirmed that both Bem1p and GIV-CT form an extensive and similar interface with Exo70—although domain C is the major contributor, domains A, B, and D are also relevant (Figures 1E–1G). Despite the overall similarity in domain contributions, combination of multiple single point mutations on the surface of Exo70p that disrupts the Bem1p•Exo70 interaction (Liu and Novick, 2014) did not seem to affect binding to GIV-CT (Figure S2B). These findings are in keeping with the fact that mammalian and yeast Exo70 differ in both conformation and surface charge (Figures 1F and S2C) and share low level of sequence conservation, which has been suggested as a basis for species-specific functions of the exocyst (Moore et al., 2007). We also believe that these findings using Exo70p truncations and multi-point mutations are possibly real and not confounded by truncation/mutation-related artifacts (protein misfolding, denaturing, etc.) because the same constructs when used in earlier studies bound Rho3-GTP (Liu and Novick, 2014).

In the absence of conserved amino acids across species, or any other structural clues, generating corresponding mutations in human Exo70 was not attempted. When we carried out competition assays with recombinant proteins to determine if the Bem1p•Exo70p and GIV•Exo70 interactions are mutually exclusive or inclusive, we found that both GIV and Bem1p could compete for yeast (Figure 1H) and human (Figure 1I) Exo70. These findings suggest that Bem1p and GIV may share the mechanism of binding and that their binding interfaces with Exo70 are either significantly overlapping or non-overlapping but pose significant steric hindrance. Regardless, these findings demonstrate that despite divergent modular makeup, both polarity scaffolds Bem1p (yeast) and GIV (mammals) can bind Exo70 via mechanisms that are shared (i.e., use of Domains C of Exo70 as major contributor). They both may use either same or distinct interfaces for binding Exo70, but nonetheless bind in a mutually exclusive manner. Although each can bind both yeast and human Exo70 proteins, they demonstrate species preference (Figure 1J).

GIV Is Required for Exo70 Localization, Polarized Exocytosis

Because GIV's role in tumor cell invasion and its ability to promote cancer metastasis has been demonstrated *in vitro* (Leyme et al., 2015; Rahman-Zaman et al., 2018; Jiang et al., 2008) and *in vivo* (Jiang et al., 2008) using MDA MB231 human breast cancer cells, we used the same cells and asked if GIV is required for the polarized delivery of cargo proteins, e.g., matrix metalloproteases that aid in tumor

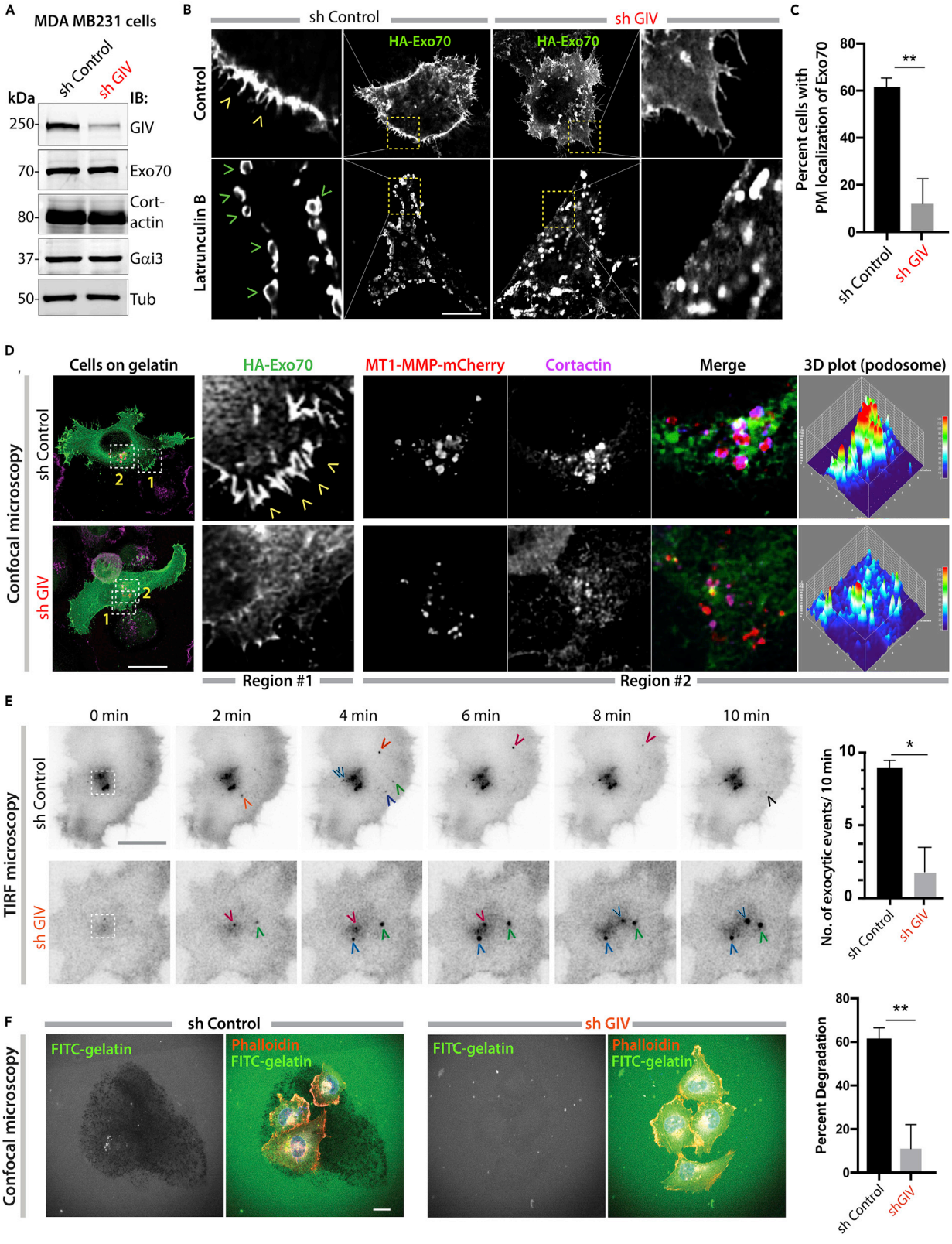
A
MDA MB231 cells
sh Control
sh GIV
kDa
IB:
250
GIV
70
Exo70
80
Cort-actin
37
Gαi3
50
Tub
B
sh Control
sh GIV
HA-Exo70
HA-Exo70
Control
Latrunculin B
C
Percent cells with PM localization of Exo70
80
60
40
20
0
**
sh Control
sh GIV
D
Cells on gelatin
HA-Exo70
MT1-MMP-mCherry
Cortactin
Merge
3D plot (podosome)
Confocal microscopy
sh Control
sh GIV
2
1
2
1
Region #1
Region #2
E
0 min
2 min
4 min
6 min
8 min
10 min
TIRF microscopy
sh Control
sh GIV
No. of exocytic events/ 10 min
10
5
0
*
sh Control
sh GIV
F
sh Control
sh GIV
Confocal microscopy
FITC-gelatin
Phalloidin
FITC-gelatin
FITC-gelatin
Phalloidin
FITC-gelatin
Percent Degradation
80
60
40
20
0
**
sh Control
shGIV

Figure 2. GIV Is Required for Exo70 Localization and Polarized Exocytosis

(A) Immunoblots of lysates of control (sh Control) and GIV-depleted (sh GIV) MDA MB231 cells.

(B) Control (sh Control) and GIV-depleted (sh GIV) MDA MB231 cells expressing HA-Exo70 were treated (bottom) or not (top) with 25 μM latrunculin B for 24 h before fixation with PFA. Fixed cells were stained for HA and analyzed by confocal microscopy. Representative deconvolved images are shown. Scale bar, 10 μm. Arrowheads, PM localization.

(C) Bar graphs show the % cells with PM localization of Exo70-HA. Error bars represent standard error of mean; ± SEM; n = ~ 30 cells/assay, 3 independent assays. **p value <0.01.

(D) Cells in (B) exogenously expressing HA-Exo70 (green) and MT1-MMP-mCherry (red) were plated on gelatin-coated coverslips and fixed and stained with the invadosome marker cortactin (magenta). Representative deconvolved images are shown. Boxed area with grey interrupted line represents cell's center, likely invadosomes. Colored arrowheads track single exocytic events. Scale bar, 10 μm. Insets were analyzed by rendering 3D surface plots using ImageJ. Cortactin/MT1-MMP colocalization was determined by Pearson's correlation coefficient reaching a value of 0.71 ± 0.05 and 0.15 ± 0.04 in control and GIV-depleted cells, respectively, from four different experiments.

(E) Cells in (B) exogenously expressing MT1-MMP-pHLuorin were plated on a layer of unlabeled gelatin and imaged by TIRF microscopy. Left: Still frames from a 10-min-long movie (Videos S1 and S2). Each colored arrowhead marks one successfully exocytosed vesicle. Scale bar, 2.5 μm. Right: Bar graph shows the number of exocytic events that were encountered during the 10-min-long movie in (D). N = ~ 5–10 cells/assay. Error bars represent standard error of mean; ± SEM. *p value <0.05.

(F) Cells in (B) were plated for 5 h on fluorescein isothiocyanate (FITC)-conjugated cross-linked gelatin (green) and then fixed and stained for F-actin (Phalloidin; red). (Left) Representative images are shown. Scale bar, 10 μm. (Right) Bar graphs display the % of cells that showed degradation of gelatin. N = ~100–200 cells/experiment × 3. Error bars represent standard error of mean; ± SEM. **p value = 0.001.

dissemination by degrading extracellular matrix (ECM). We first confirmed that depletion of GIV (~85% depletion by small hairpin RNA [shRNA]; Figure 2B) does not change the levels of Exo70 or cortactin; the latter is a marker of invadosomes, which are subcellular actin-rich landmarks that are specialized for matrix degradation because of polarized exocytosis of proteinases (Castro-Castro et al., 2016; Hoshino et al., 2013). We found that hemagglutinin (HA)-tagged Exo70 localized to the PM in control but not GIV-depleted cells (Figures 2B and S3A, top panel). In control cells, disruption of actin cytoskeleton with latrunculin B, a chemical that has been widely used for its ability to sequester G-actin and prevent F-actin assembly (Morton et al., 2000), prevented fusion of Exo70-positive vesicles but did not impact their docking at specific sites on the PM; in GIV-depleted cells the vesicles were in disarray (Figures 2B and S3A, bottom panel; Figure 2C). These findings indicate that GIV is required for the localization of Exo70 to the PM and that such localization is actin independent.

Next, to analyze how Exo70 localization may impact polarized exocytosis of proteases to invadosomes, we co-transfected the MDA MB231 cells with HA-Exo70 and a previously validated MT1-MMP-mCherry construct (Steffen et al., 2008), plated them on gelatin, and looked for the co-localization of MT1-MMP, Exo70, and cortactin. Again, HA-Exo70 localized to the PM in the presence of GIV, but significantly less in its absence (Figure 2D; Region #1). Colocalization between MT1-MMP-mCherry and cortactin was easily detected in control cells, but significantly reduced in cells without GIV (Figures 2D and S3B; Region #2 and 3D plot of invadosome). These findings indicate that GIV is required for efficient localization of proteases near invadosomes. We also noted that despite similar levels of expression of cortactin in the GIV-depleted cells (Figure 2A), the localization of cortactin at the sub-nuclear plane at the center of these cells was consistently impaired (Figure 2D). To assess the dynamics of polarized exocytosis in real time, we used a pH-sensitive MT1-MMP-pHluorin construct (Monteiro et al., 2013), which is fluorescent only at an extracellular pH of 7.4. Prior studies using this construct and total internal reflection fluorescence (TIRF) live-cell microscopy have demonstrated that MT1-MMP-pHluorin demonstrates dot-like localization at the substrate-attached cell side, reminiscent of invadosomes (El Azzouzi et al., 2016; Planchon et al., 2018). When we carried out TIRF microscopy on control and GIV-depleted MDA MB231 cells, we found that the number of exocytic events were significantly lower in the latter (Figure 2E; Videos S1 and S2), and that they were not clustered near the center of the cell (Figure 2E; interrupted white square). Consistent with these findings, compared with controls cells fewer % of GIV-depleted cells demonstrated gelatin degradation (Figure 2F). Together, these findings suggest that GIV is required for the localization of Exo70 to specific sites at the PM, and for the polarized exocytosis of MT1-MMP at the invadosomes. Because the polarized exocytosis of MT1-MMP and the formation, maturation, and functions of the invadosome (which is marked by cortactin) are known to be intertwined (Juin et al., 2012; Monteiro et al., 2013; Castro-Castro et al., 2016; Castagnino et al., 2018; Artym et al., 2006), our findings also suggest that GIV-dependent exocytosis of the protease may impact the dynamics of invadosomes and efficient degradation of ECM.

A Short Linear Motif on C Terminus Mediates GIV's Interaction with Exo70

To pinpoint the role of GIV in polarized exocytosis, we set out to identify mutant(s) of GIV that may not bind Exo70. Previously, using domain mapping studies the Exo70p-binding domain of Bem1p was narrowed

down to amino acids 309–510, which includes three-quarters of the PX domain, half of the PB1 domain, and the region connecting them (see Figure 1A) as both necessary and sufficient (Liu and Novick, 2014). Because Bem1p and GIV appeared to share the mechanism of binding to Exo70, via what appears to be extensive binding interfaces (Figures 1H and 1I), we hypothesized that the interactions could be sensitive to some key residues. When Bem1p and GIV aligned, we noticed that they have very little similarity in sequences, except for a short stretch of sequence within the PX domain of Bem1p, ^{320}DFYD^{323} (Figures 3A and 3B). When we superimposed two previously solved structures of Bem1p, we noted that the phenylalanine (F) within this sequence exhibits flexibility (Figure 3A). We targeted this putative short linear interaction motif (SLIM, ^{1741}DFYD^{1744}) in GIV either by selectively replacing the Phe > Ala (F^{1742}A) or by replacing the motif with Ala at three of the four positions (AAxA). Both mutants did not bind GST-Exo70 (Figure 3C). Next we carried out a series of mutations within and flanking the SLIM and noted that several of them impaired binding of GIV to Exo70 (Figure 3D), demonstrating that regardless of potentially extensive contact sites, the GIV•Exo70 interaction is sensitive to point-directed mutagenesis.

The sequence alignment also predicted mutations that would improve GIV's ability to bind yeast Exo70p (i.e., R^{1745}L) or those that might impair Bem1p's ability to bind Exo70p (F^{321}A) (Figure 3E). We found both predictions to be true—a mutant GIV (R^{1745}L) bound Exo70p stronger than GIV-wild-type (WT) (Figures 3F and S4A). Similarly, the F321A mutant Bem1p did not bind Exo70p (Figure 3G). These findings provide further evidence that although the interactions between GIV or Bem1p is complex and may occur via an extensive interface, and that the mechanisms of these interactions in yeast and mammals are divergent for the most part, the SLIM we identified in this work may represent an evolutionary conserved mechanism (Figure S4B). This Exo70-binding SLIM, localized within the C terminus of GIV, adds to the gathering catalog of SLIMs used by GIV to scaffold diverse signaling components (Figure S4C).

Exo70 Binding-Deficient GIV Mutant Fails to Deliver MT1-MMP to Invadosomes

We next asked if the phenotypes we observed previously (Figure 2) were because of GIV's ability to bind Exo70. To this end, we generated MDA MB231 cell lines in which endogenous GIV was depleted by shRNA before being restored with full-length GIV either WT or the Exo70 binding-deficient GIV mutant AAxA (Figure 4A) and used them in similar assays as before. We found that compared with cells expressing GIV-WT, those expressing the binding-deficient AAxA GIV mutant showed impaired localization of HA-Exo70 at the PM (Figure 4B); colocalization of both Exo70 and MT1-MMP-mCherry to cortactin-positive invadosomes (Figure 4C); rate of exocytic events, as determined by TIRF microscopy on cells expressing MT1-MMP-pHluorin (Figures 4D and 4E; Videos S3, S4, and S5); and gelatin degradation (Figures 4F and 4G). These results were also validated using another Exo70-binding deficient mutant, F^{1742}A (Figures S5A–S5C and S6). Key findings were also reproduced in HeLa cells (Figures S7A–S7C), which have been widely used in the past decade as the cellular model system of choice to study GIV's functions. These findings indicate that the GIV•Exo70 interaction may be critical for the localization of Exo70 to vesicle tethering sites at the PM and for the polarized exocytosis of MT1-MMP proteases at or near the invadosomes of cells.

Cells Expressing the Exo70-Binding-Deficient Mutant GIV Fails to Spread, Degrade Matrix, and Invade

Next we asked how the GIV•Exo70 interaction impacts cellular phenotypes that have been previously attributed to exocytosis of either membrane or proteases, e.g., cell spreading and invasion through the basement membrane ECM, but not impact adhesion; the latter is primarily mediated by integrins and is independent of exocytosis (Figure 5A). We hypothesized that cells expressing a mutant GIV that cannot bind Exo70 may adhere normally but may not spread or invade efficiently through the ECM. Cell adhesion assays confirmed that depletion of GIV impairs adhesion on collagen-coated surface (Figure 5B), which is in keeping with prior work by others and us showing that GIV modulates integrin signaling (Leyme et al., 2015, 2016; Lopez-Sanchez et al., 2015a). Cells expressing either GIV-WT or the binding-deficient GIV-AAxA mutant adhered to the collagen to similar extents as control cells (Figure 5B), indicating that the cell adhesion occurs independent of the GIV•Exo70 interaction. As for cell spreading, we analyzed spreading at or beyond ~30 min, a phase of spreading that requires membrane exocytosis and is proteolysis dependent (Figure 5C). We found that although both GIV-WT and GIV-AAxA cells adhered equally well to collagen-coated surfaces (Figure 5B), the latter showed significant impairment in cell spreading (Figures 5D and 5E), indicating that cell spreading requires an intact GIV•Exo70 interaction. Haptotaxis assays carried out across a 0% to 10% serum gradient (Figure 5F) showed that depletion of GIV impairs cell invasion; however, such impairment is rescued by GIV-WT, but not the Exo70 binding-deficient GIV-AAxA mutant

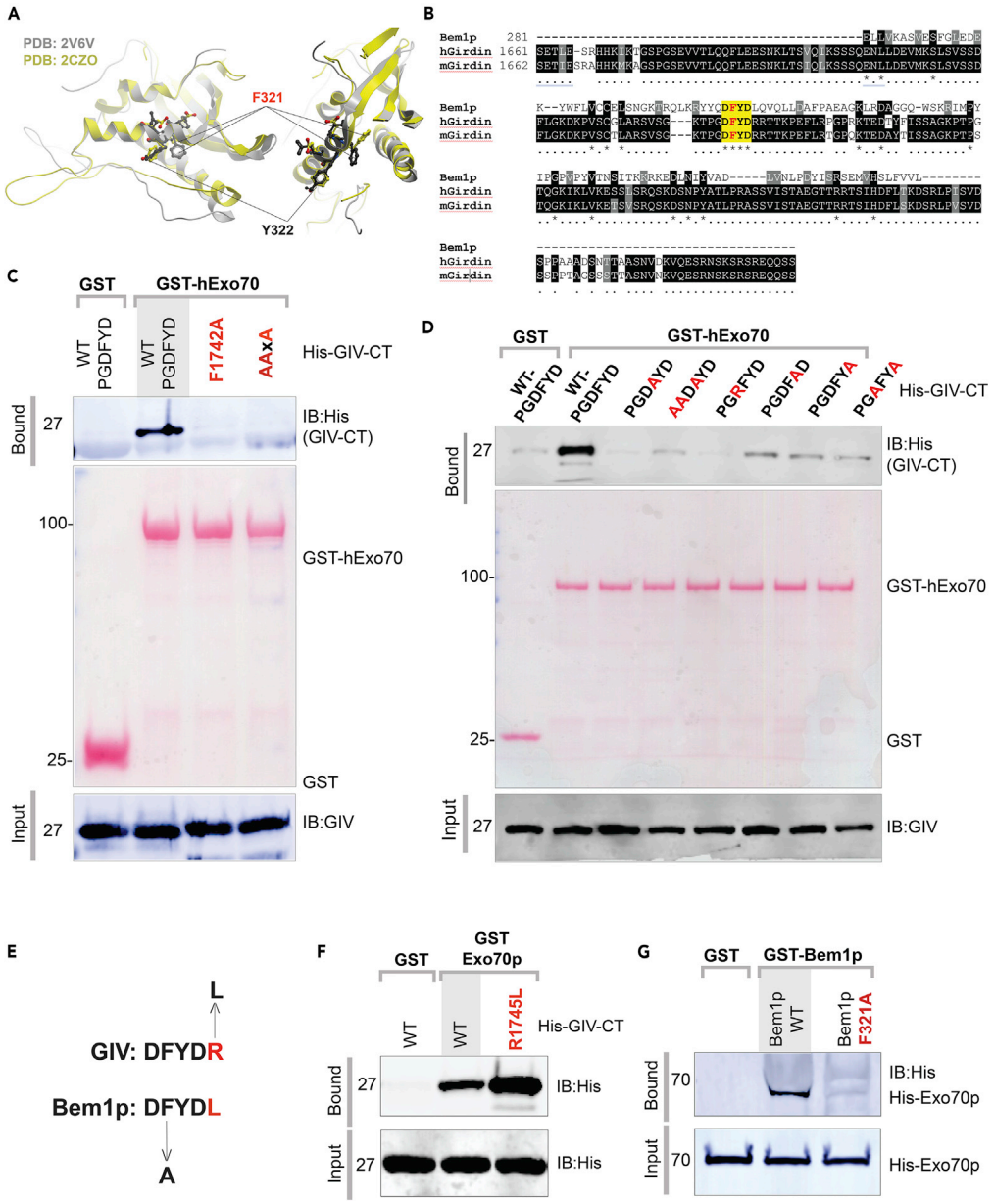

Figure 3. A Short Linear Motif on C Terminus Mediates GIV's Interaction with Exo70

(A) Two views of the two solved crystal structures of PX domain of Bem1p (PDB:2V6V, Stahelin et al., 2007; PDB:2CZO, unpublished), showing the position and orientation of key residues Phe (F)321 and Tyr (Y)322 on Bem1p that are within the previously identified stretch of amino acids 309–510 that is both necessary and sufficient for binding to Exo70p.

(B) Sequence alignment showing a short linear "DFYD" motif that is conserved between GIV and Bem1p.

(C and D) Recombinant WT and mutant His-GIV-CT (~3 μg) proteins were used in GST pull-down assays with GST or GST-hExo70 (human). Two mutants in panel C are used throughout the remaining study to investigate the role of the GIV-Exo70 interaction. Other mutants in panel D were used to characterize the Exo-70-binding motif on GIV. Bound GIV was visualized by immunoblotting (IB) using anti-His monoclonal antibody (mAb). Equal loading of GST proteins was confirmed by Ponceau S staining.

(E) Sequence-based prediction of mutations in GIV (top; R1742»L) and Bem1p (bottom; F312»A) that should enhance and reduce binding to GST-Exo70p (yeast), respectively.

(F) Recombinant His-GIV-CT WT or R1742»L mutant was used in GST pull-down assays with GST or GST-hExo70 (human). Bound GIV was visualized by immunoblotting using anti-His mAb.

(G) Recombinant His-Exo70p was used in GST pull-down assays with GST or GST-Bem1p WT or F312»A mutant. Bound Exo70p was visualized by immunoblotting using anti-His mAb.

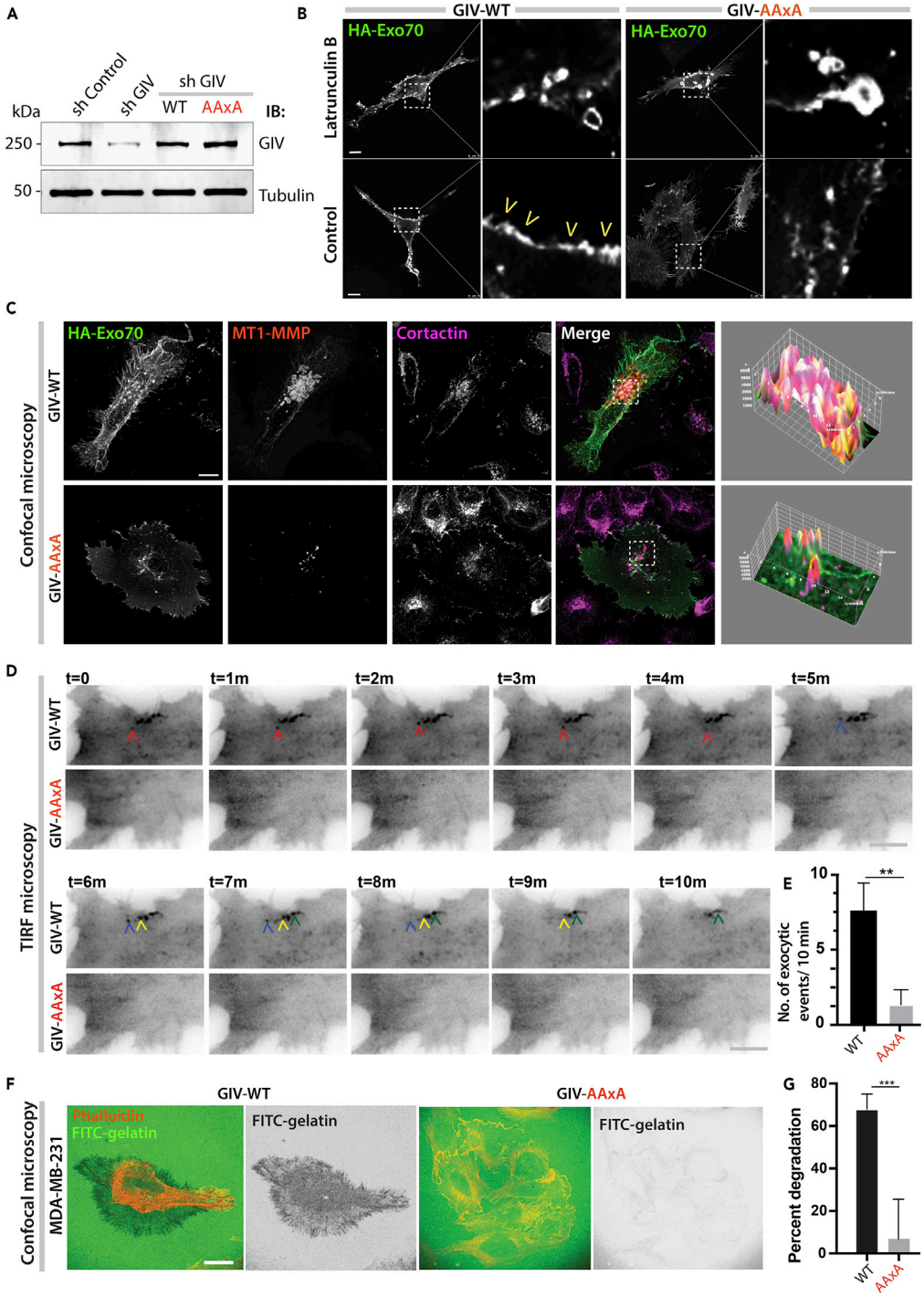

Figure 4. Exo70-Binding-Deficient Mutant GIV Fails to Deliver MT1-MMP to Invadosomes

(A) Immunoblots of lysates of control (sh Control) and GIV-depleted (sh GIV) MDA MB231 cells stably expressing GIV-FLAG WT and exo70-binding deficient AAxA mutant constructs. See also Figure S5A.

(B) GIV-depleted (sh GIV) MDA-MB-231 cells stably expressing GIV-WT or GIV-AAxA mutant were transfected with HA-Exo70 and were either treated (top) or not (bottom) with 25 μM latrunculin B for 24 h before fixation with PFA. Fixed cells were stained for HA and analyzed by confocal microscopy. Representative deconvolved images are shown. Arrowheads, PM localization. Unusually large membrane vesicles (see inset) were noted in mutant cells, but PM localization was impaired. Scale bar, 10 μm.

Figure 4. *Continued*

(C) Cells in (B) transfected with HA-Exo70 (green) and MT1-MMP-mCherry (red) were plated on gelatin-coated coverslips, fixed, and stained with the invadosome marker cortactin (magenta). Representative deconvolved images are shown. Insets were analyzed by rendering 3D surface plots using ImageJ. See also Figure S5B for F1742A mutant GIV. Cortactin/MT1-MMP colocalization was determined by Pearson's correlation coefficient reaching a value of 0.87 ± 0.07 and 0.35 ± 0.02 in GIV-WT and GIV-AAxA cells, respectively, from three different experiments. Scale bar, 10 μm.

(D) Cells in (B) were transfected with MT1-MMP-pHLuorin and were plated on a layer of unlabeled gelatin and imaged by TIRF microscopy. Each colored arrowhead tracks one vesicle. Still frames from a 10-min-long movie (Videos S3 and S4). Scale bar, 2.5 μm. See also Figure S5C for F1742A mutant GIV.

(E) Bar graph shows the number of exocytic events that were encountered during the 10-min-long movie in (D). N = ~ 5–10 cells/assay. Error bars represent standard error of mean; ± SEM. **p value = 0.01.

(F) Cells in (B) were plated for 5 h on FITC-conjugated cross-linked gelatin (green) and then fixed and stained for F-actin (Phalloidin; red). Representative images are shown. Scale bar, 10 μm. See also Figure S6 for F1742A mutant GIV.

(G) Bar graphs display the % of cells that showed degradation of gelatin. N = ~100–200 cells/experiment × 3. Error bars represent standard error of mean; ± SEM. ***p values = 0.001.

(Figures 5G and 5H). These findings demonstrate that the GIV•Exo70 interaction is required for key phenotypes of cancer cells that require efficient polarized exocytosis of proteases that degrade the ECM and aid in tumor dissemination.

Components of Polarized Exocytosis Synergize during Tumor Metastasis

We next asked if the interaction between GIV and Exo70 we report here and the impact of such interaction on the invasive properties of tumor cells can be meaningful when assessing tumor behavior and/or prognosticating clinical outcome. To discern if the levels of expression of Exo70 or GIV alone could impact one of the most important readouts of cancer aggressiveness, i.e., metastasis-free patient survival, we chose to study a pooled cohort of patients (GSE2034, GSE2603 and GSE12276; Minn et al., 2005; Bos et al., 2009; Wang et al., 2005) with breast cancers. These cohorts are unique because the patients did not receive adjuvant chemotherapy, and hence, metastatic progression in them reflects natural disease progression and not resistance/selection under treatment. Samples were divided into "low" and "high" subgroups with regard to Exo70 (EXOC7) and GIV (CCDC88A) gene expression levels using the StepMiner algorithm (Sahoo et al., 2007), implemented within the hierarchical exploration of gene expression microarrays online (HEGEMON) software (Dalerba et al., 2011; Volkmer et al., 2012). Kaplan-Meier analyses of the disease-free survival showed that Exo70 and GIV had opposing impact on outcome (Figure 6A)—high levels of GIV expression carried a grave prognosis, i.e., a shorter metastasis-free survival, which is consistent with numerous prior studies (reviewed in Ghosh, 2015). By contrast, high expression of Exo70 carried a better prognosis, i.e., a longer metastasis-free survival (Figure 6A); this is also consistent with prior findings that an epithelial isoform of Exo70, which is the isoform that is primarily responsible for exocytic secretions, inhibits tumor metastasis in mice (Lu et al., 2013).

We next sought to determine if the levels of expression of either GIV or Exo70 and other genes that encode major polarity scaffolds (Lin et al., 2015) interact synergistically as independent variables to impact survival of patients. To this end, we carried out a Cox proportional hazards model (Cox, 1972), which is a regression model that is commonly used as a statistical method for investigating the effect of several variables upon the time it takes for a specified event to happen, in this case, metastasis. We found that besides GIV/CCDC88A, Exo70 significantly and negatively interacts with multiple members of the Par, Scribble, and Crumbs family of polarity scaffolds (Figure 6B), in that, high levels of expression of each of these scaffolds in the setting of high Exo70 expression was sufficient in shortening metastasis-free survival. Of all those polarity scaffolds that interacted with Exo70, only DLG5 continued to show positive synergistic interactions with CCDC88A (GIV) (Figure 6C), in that, high levels of expression of DLG5 in the setting of high GIV expression further shortened metastasis-free survival. Next we asked how Exo70 or GIV interacts with other components of the exocytic machinery, i.e., core trafficking components (i.e., monomeric GTPases Rabs, Arf6), focal adhesions cytoskeleton and Rho GTPases (Paxillin, PXN; Actin, ACTB; TC10, RHOQ; Rho-associated kinase, ROCK1), cargo (MT1-MMP, MMP14), and receptors (ITGB1 and EGFR). We found that whereas many components may negatively interact with Exo70 (Figure 6D), only TC10 GTPase (RHOQ) positively and synergistically interacts with GIV to shorten metastasis-free survival (Figure 6E).

Based on all gene pairs tested, we computed the interactome for Exo70 that shortens metastasis-free survival (Figure 6F). The interactome enabled two major predictions. (1) Polarized exocytosis during metastasis may require Exo70 to synergize with both GIV and DLG5. Because GIV binds DLG5 and their

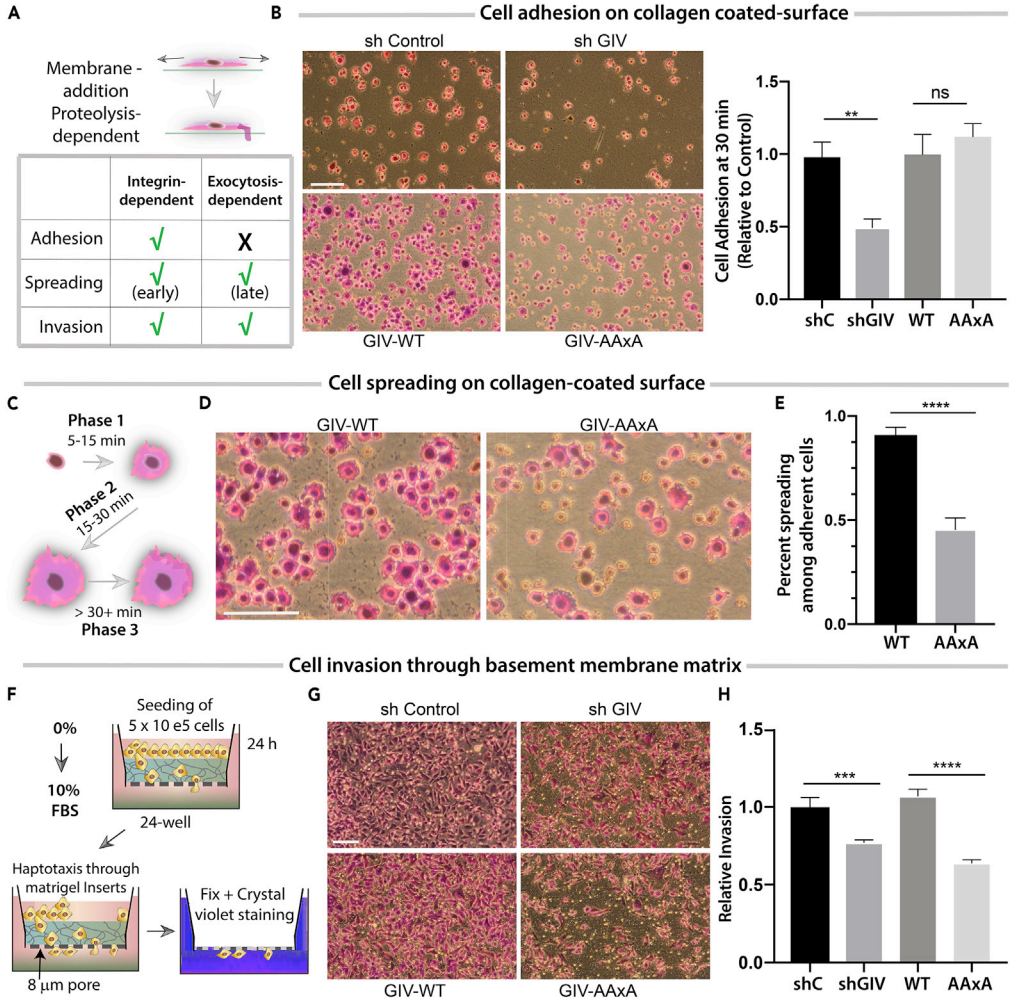

Figure 5. Cells Expressing Exo70-Binding-Deficient Mutant GIV Adhere, but Fail to Spread, Degrade Matrix, and Invade

(A) Schematic summarizing how polarized exocytosis of membrane and cargo (in this case MT1-MMP) impacts cell adhesion, spreading, and invasion. Check, dependent; cross, independent.

(B) MDA-MB 231 cell lines were analyzed for cell adhesion by growing on poly-D-lysine-coated surface, resuspending, and then plating on 12-well collagen-coated plates for 30 min before fixing with 4% PFA and staining with crystal violet. Cells were visualized and imaged by light microscopy. (Left) Representative images are shown. Scale bar, 250 µm. (Right) Bar graphs display the relative numbers of adherent cells per field, as determined using ImageJ. Error bars represent standard error of mean; ± SEM (n = 4); **p value < 0.01; ns, not significant.

(C) Schematic summarizing the phases of cell spreading during adhesion.

(D) Adherent MDA-MB 231 cells in (B) were further analyzed for attachment-induced cell spreading at higher magnification. Representative images are shown. Scale bar, 250 µm.

(E) Bar graphs display the quantification of % spreading in (D). Error bars represent standard error of mean; ± SEM (n = 4); ****p value < 0.0001.

(F) Schematic diagram showing the serum gradient-induced haptotaxis assay conditions used in (G and H).

(G) MDA-MB 231 cell lines in (A) were analyzed for the ability to invade through Matrigel-coated transwells. The number of cells that successfully invaded within 24 h was imaged. Representative images are shown. Scale bar, 250 µm.

(H) Bar graphs display the number of invading cells in (G), as determined using ImageJ. Error bars represent standard error of mean; ± SEM (n = 4); ***p value < 0.001, ****p value < 0.0001.

interaction regulates the formation of invadopodia (Ke et al., 2017), and DLG5 in turn engages with tSNARE syntaxin-4 (Nechiporuk et al., 2007) to enable the exocytosis (Wang et al., 2014), it is possible that DLG5 also impacts polarized exocytosis. (2) The interactome predicted that TC10, a close relative of Cdc42 is a likely candidate Rho-superfamily GTPase that may cooperate with GIV during the exocytosis of MT1-MMP.

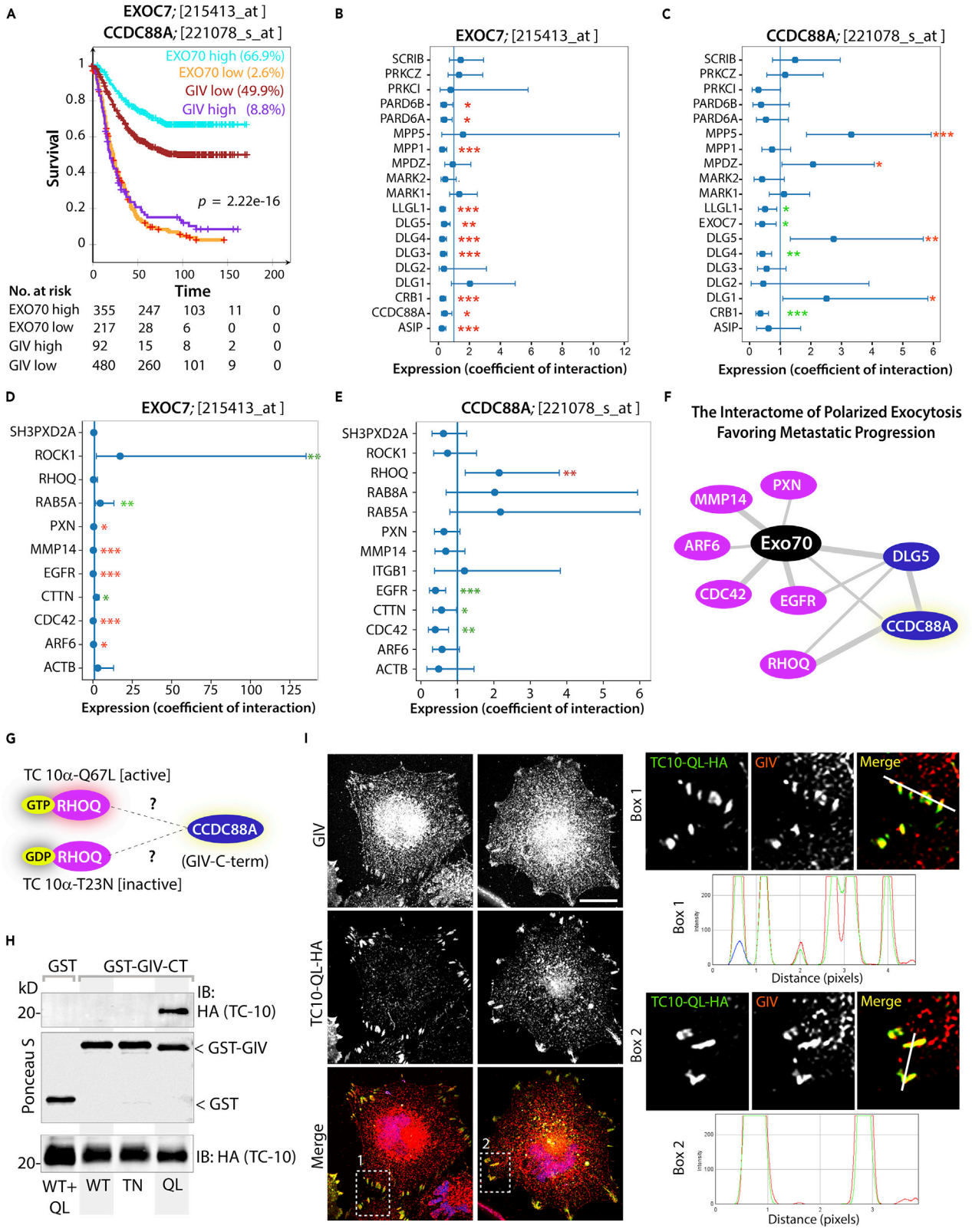
A
EXOC7; [215413_at]
CCDC88A; [221078_s_at]
EXO70 high (66.9%)
EXO70 low (2.6%)
GIV low (49.9%)
GIV high (8.8%)
Survival
p = 2.22e-16
Time
No. at risk
EXO70 high 355 247 103 11 0
EXO70 low 217 28 6 0 0
GIV high 92 15 8 2 0
GIV low 480 260 101 9 0
B
EXOC7; [215413_at]
SCRIB
PRKCZ
PRKCI
PARD6B
PARD6A
MPP5
MPP1
MPDZ
MARK2
MARK1
LLGL1
DLG5
DLG4
DLG3
DLG2
DLG1
CRB1
CCDC88A
ASIP
Expression (coefficient of interaction)
C
CCDC88A; [221078_s_at]
EXOC7
Expression (coefficient of interaction)
D
EXOC7; [215413_at]
SH3PXD2A
ROCK1
RHOQ
RAB5A
PXN
MMP14
EGFR
CTTN
CDC42
ARF6
ACTB
Expression (coefficient of interaction)
E
CCDC88A; [221078_s_at]
RAB8A
ITGB1
Expression (coefficient of interaction)
F
The Interactome of Polarized Exocytosis Favoring Metastatic Progression
PXN
MMP14
ARF6
Exo70
DLG5
CDC42
EGFR
CCDC88A
RHOQ
G
TC 10α-Q67L [active]
GTP
RHOQ
?
CCDC88A
GDP
RHOQ
?
(GIV-C-term)
TC 10α-T23N [inactive]
H
GST
GST-GIV-CT
kD
20-
IB:
HA (TC-10)
Ponceau S
< GST-GIV
< GST
20-
IB: HA (TC-10)
WT+ QL
WT
TN
QL
I
GIV
TC10-QL-HA
Merge
1
2
TC10-QL-HA
GIV
Merge
Box 1
Box 1
Intensity
Distance (pixels)
Box 2
Box 2
Intensity
Distance (pixels)

Figure 6. Polarity Scaffold GIV (CCDC88A), Matrix Metalloprotease MT1-MMP, and Exocyst Complexes Synergize during Metastasis

(A) An overlay of Kaplan-Meier curves for metastasis-free survival over time among 572 patients (3 independent cohorts, pooled, Minn et al., 2005; Bos et al., 2009; Wang et al., 2005) who did not receive adjuvant therapy segregated into high versus low levels of exo70 (EXOC7) or GIV (CCDC88A) in primary tumors.

(B and C) Statistical interaction (synergy between variables) is measured in the Cox proportional hazards regression model for EXOC7 (exo70) (B), CCDC88A (GIV) (C), and all mammalian polarity scaffold proteins, including CCDC88A (GIV). Coefficient of the interaction term in Cox regression models is plotted with 95% confidence interval that demonstrates the significance of the statistical interaction. *p = 0.05, **p = 0.01. Red and green asterisks denote shorter or longer metastasis-free survival, respectively.

(D and E) Statistical interaction (synergy between variables) is measured in the Cox proportional hazards regression model as in (B and C) for EXOC7 (exo70) (D), CCDC88A (GIV) (E), and mammalian proteins known to be involved in or influence the exocytosis of MT1-MMP. Red and green asterisks denote shorter and longer metastasis-free survival, respectively.

(F) Schematic summarizing only those interactions with EXOC7 that reduced metastasis-free survival. Purple, genes that encode polarity proteins; pink, others. Network-based prediction of RHOQ (TC10) as the RHO GTPase counterpart in mammals that synergistically interacts with CCDC88A (GIV).

(G and H) (G) Schematic summarizing the constructs used in (H) to assess nucleotide state-dependent interaction between TC10 and GIV. GST pull-down assays were carried out using lysates of COS7 cells as source of TC10-HA WT or constitutively active (QL) or inactive (TN) mutants with GST or GST-GIV-CT. Bound proteins were assessed with anti-HA mAb.

(I) MDA MB231 cells exogenously expressing TC10-WT-QL (green) were fixed and stained for endogenous GIV (red). Representative images of transfected cells are shown. Scale bar, 10 μm. Red and green panels are shown in gray scale. Insets (Box1, 2) were analyzed for colocalization by line scans to generate RGB plots using ImageJ. TC-10/GIV colocalization was determined by Pearson's correlation coefficient reaching a value of 0.86 ± 0.06 from three different cultures.

We asked if GIV's C terminus interacts with TC10 and if such interaction is regulated by its nucleotide-bound (activity) state. Using previously validated TC10 constructs (Chiang et al., 2002) that mimic active (QL) or inactive (TN) conformations (Figure 6G) in pull-down assays with GST-GIV-CT we first confirmed that GIV exclusively binds active, but not the inactive, GTPase (Figure 6H). To translate the relevance of these *in vitro* findings to cells, we tested the impact of TC10 on the localization of endogenous full-length GIV, as determined by confocal immunofluorescence on fixed cells. Transfection of active QL mutant, but not WT TC10, was sufficient to enhance the localization of GIV to focal adhesion and/or invadosome-like peripherally located structures (Figures 6I and S8), where they colocalized (Figure 6I, RGB plots). These findings are in keeping with the fact that mammalian Exo70 has been shown to directly interact with active TC10 (Inoue et al., 2003) and that activation of TC10 has been linked with the formation and functions of the invadosome. Together, our findings suggest that TC10 may be the evolutionary counterpart that binds GIV, and in doing so, may fulfill the role that cdc42p has been shown to perform alongside the Exo70p•Bem1p complex in yeast (Liu and Novick, 2014).

Conclusions

The major discovery we report herein is the mechanism and consequences of a direct interaction between GIV and Exo70, and its impact on polarized exocytosis of matrix metalloprotease MT1-MMP. Using selective single point mutants of GIV that are incapable of binding Exo70, we chart the two major consequences of this GIV•Exo70 interaction. First, the GIV•Exo70 interaction impacts our understanding of exocytosis in mammalian cells. Findings reveal that GIV imparts polarization to the process of exocytosis. How does GIV do so? Previously, we showed that GIV's ability to activate trimeric GTPase Gαi is critical for its ability to enhance insulin-stimulated exocytosis of glucose transporter, GLUT4-storage vesicles (Lopez-Sanchez et al., 2015b), which in part accounts for GIV's ability to maintain insulin sensitivity in skeletal muscle cells (Ma et al., 2015). Others have demonstrated that the same G protein regulatory module is essential for GIV's ability to activate Par3/6/aPKC polarity complexes (Sasaki et al., 2015). Because the Par3/6/aPKC complexes are highly versatile in their ability to orchestrate all forms of cell polarity, e.g., front-rear, apical-basal, planar cell, and polarity during migration (Suzuki and Ohno, 2006), and positive feedback loop signals are essential for the amplification of stochastically arising clusters of polarity factors that create and maintain such forms of polarity (Mccaffrey and Macara, 2012), we propose that GIV enables polarized exocytosis in a bipartite manner: its ability to bind Exo70 imparts polarity and its ability to activate the Par3/6/aPKC polarity complexes via G protein intermediates (i.e., "free" $G\beta^{\gamma}$ dimers) serves as the positive feedback loop. Furthermore, GIV has been shown to use "free" $G\beta^{\gamma}$ intermediates to activate Rho-GTPases (Leyme et al., 2015) and to terminate Arf-GTPase signaling on endomembranes (Lo et al., 2015), which may serve as additional positive and negative feedback loops. Such feedback loops have been shown to be critical for imparting robustness to the process of polarized exocytosis in yeast (Howell et al., 2012): a positive feedback occurs wherein Cdc42p•GTP at the membrane can recruit the cytoplasmic Bem1p complex, which generates more Cdc42p•GTP from local Cdc42p•GDP by GEF-catalyzed exchange; a negative feedback loop enables dispersal of the polarity complexes by affecting the duration of activation of Cdc42p•GTP or phosphoinhibition of Bem1p. Whether GIV is at the crossroads of these regulatory loops

with the Rho-GTPase TC10 or Rab/Arf-GTPases and what might be the exact mechanism(s) that impart regulatory control and robustness to the mammalian polarized exocytic machinery remain unknown. Regardless, GIV's multi-modular makeup (see Figure 1A), its functional diversity (Aznar et al., 2016a), its growing catalog of phosphomodifications (including the "Y" within the Exo70-binding DFY^{1743}D motif, see Figure 3; phosphosite.org), and its ability to integrate signals at the cross-roads of diverse types of signaling pathways (reviewed in Ghosh et al., 2017) tempts us to speculate that its association with Exo70 may impose intricate regulatory control over the mammalian polarized exocytic machinery making it more precise, context-dependent, versatile, and adapted to the needs of multi-cellular organisms. In keeping with this assumption, it is noteworthy that the yeast polarity scaffold Bem1p has no known homologs in any multicellular organisms (Liu and Novick, 2014), whereas GIV (Coleman et al., 2016) and its associated aPKC/Par3/6 complexes (Thompson, 2013) are absent in yeast and co-evolved only in worms and flies and highly conserved in mammals. Thus, our findings reveal the extent of evolutionary divergence in the polarized exocytic machinery from yeast to mammals (see legend, Figure 7); although the octameric exocyst complex remained constant, each component in yeast is replaced by its functional counterpart in mammals, beginning with an abrupt change in the polarity determinant coinciding with the onset of multicellular life forms. Although our findings suggest that the GIV•Exo70 co-complex may constitute the core component that imparts polarity to exocytosis, these may not be sufficient. It is noteworthy that just like Bem1p is not the only component affecting Exo70 localization in yeast ($PI_{4,5}P_2$, Cdc42, Rho1 and actin all play significant roles), GIV may not be the only component affecting polarized exocytosis in mammalian cells and Par/aPKC complexes, TC10, actin, and others may contribute significantly.

Second, the GIV•Exo70 interaction impacts our understanding of the pro-metastatic role of GIV in diverse cancers and how it impacts key tumor cell behaviors that are dependent on proteolysis. Because GIV modulates integrin/FAK signaling via G protein intermediates (Leyme et al., 2015, 2016; Lopez-Sanchez et al., 2015b), and because integrins and MT1-MMPs regulate each other's activity, trafficking, and signaling to integrate events in the extracellular milieu (Gonzalo et al., 2010; Das et al., 2017; Baciu et al., 2003; Galvez et al., 2002; Zigrino et al., 2001; Shi and Sottile, 2011), it is possible that GIV's C terminus may help in such process of integration. However, to begin to entertain that possibility or test it, an in-depth insight into how GIV binds integrins and how such binding impacts the GIV•Exo70 interaction is required first. Another issue that remains unexplored here is how the GIV•Exo70 complex may be dysregulated in cancers. Increased tyrosine-based signaling and hyperphosphorylation of GIV at Y1743 may impact the GIV•Exo70 interaction directly. Alternatively, because both GIV (Puseenam et al., 2009; Ghosh et al., 2010) and Exo70 (Lu et al., 2013) have been shown to have alternative isoforms, pre-mRNA splicing may derail the GIV•Exo70 interaction or alter its functions indirectly. For example, in the case of Exo70, unlike the epithelial isoform that inhibits tumor metastasis, a mesenchymal isoform aids in tumor metastasis in an exocytosis-independent manner (Lu et al., 2013); the latter promotes tumor cell invasion by interacting with the Arp2/3 complex and stimulating actin branching in lamelipodia and invadopodia. Because GIV is a *bona fide* actin remodeler that impacts actin dynamics (Jiang et al., 2008; Enomoto et al., 2005), it is possible that the GIV•(mesenchymal)Exo70 complex may collaboratively enhance these actin-based processes.

LIMITATIONS OF THE STUDY

As for the limitations of this study, although we used MT1-MMP as an example of a cargo in our experiments, GIV's ability to regulate such a fundamental component of exocytosis (Exo70) may affect the exocytosis of other cargo proteins, which extend beyond transmembrane proteases, such as receptors (e.g., RTKs and integrins) and other soluble cargo proteins. Although defining the complete inventory of the impacted cargo proteins is beyond the scope of this work, ongoing proteomics/metabolomics-based studies are expected to unravel that list. Similarly, we have not delineated the exact mechanism and dynamics of the interplay between MT1-MMP, TC10, cortactin, and GIV and how that impacts invadosome formation, function, and turnover; because GIV is an actin remodeler (Jiang et al., 2008; Enomoto et al., 2005), it is likely that GIV may have a significant effect on the functions of multiple components that coordinately regulate this critical structure used by invasive cancer cells.

In conclusion, this work not only sheds light into GIV's ability to enhance a key process that aids metastasis (i.e., polarized exocytosis of matrix metalloproteases) but also reveals how the modular makeup and functional diversity of GIV imparts the process of exocytosis features beyond polarity; it represents an evolutionary advancement of the process by adding layers of regulatory control by diverse signaling pathways.

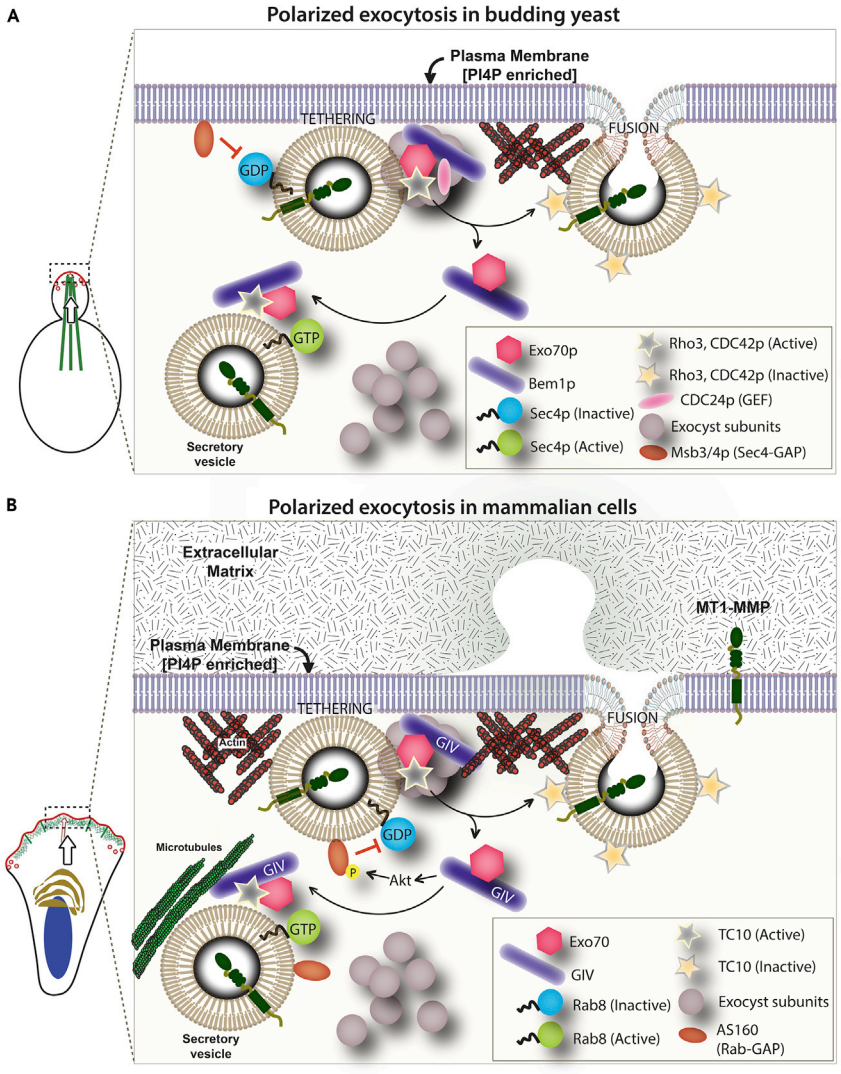

Figure 7. Components of Polarized Exocytosis Display an Evolutionary Advancement from Yeast to Mammals

(A and B) Schematics summarizing the components of exocytosis in yeast (A) and mammals (B). Mammalian counterparts of all yeast components are represented using the same symbols. The octameric exocyst complex is conserved, whereas the polarity scaffolds Bem1p and GIV are divergent, alongside the previously annotated key components of the exocytic machinery. sec4p in yeast is replaced by Rabs in mammals, whereas the sec4p GAP (Msb2/3p) is replaced by the corresponding Rab-GAP, AS160, which has been previously shown to be activated by the GIV-dependent Class 1 PI3K » Akt signaling cascade (Ma et al., 2015).

Resource Availability

Lead Contact

Pradipta Ghosh, M.D. can be contacted for all correspondence related to this manuscript via email (prghosh@ucsd.edu).

Materials Availability

Any materials generated and used in this study are available for dissemination to others.

Data and Code Availability

This study did not generate datasets.

METHODS

All methods can be found in the accompanying Transparent Methods supplemental file.

SUPPLEMENTAL INFORMATION

Supplemental Information can be found online at https://doi.org/10.1016/j.isci.2020.101246.

ACKNOWLEDGMENTS

This paper was supported by NIH CA238042, AI141630, CA100768, and CA160911 (to P.G). C.R was supported by an NCI/NIH-funded Cancer Therapeutics Training (CT2) Training Program (T32 CA121938) and an NIDDK/NIH-funded training grant (T32 DK007202). We thank Ying Dunkel and Nina Sun for technical support in this work.

AUTHOR CONTRIBUTIONS

C.R., N.R., I.-C.L., and P.G. designed, executed, and analyzed most of the experiments in this work. P.N. provided critical tools (Bem1p and Exo70p) and guidance on experimental design. D.S. carried out multivariate analysis on the impact of gene expression on metastatic progression. C.R. and P.G. conceived the project, wrote materials and methods, and edited the manuscript. P.G. wrote the manuscript.

DECLARATION OF INTERESTS

The authors declare no competing interests.

Received: November 28, 2019
Revised: April 20, 2020
Accepted: June 3, 2020
Published: July 24, 2020

REFERENCES

Artym, V.V., Zhang, Y., Seillier-Moiseiwitsch, F., Yamada, K.M., and Mueller, S.C. (2006). Dynamic interactions of cortactin and membrane type 1 matrix metalloproteinase at invadopodia: defining the stages of invadopodia formation and function. Cancer Res. *66*, 3034–3043.

Aznar, N., Kalogriopoulos, N., Midde, K.K., and Ghosh, P. (2016a). Heterotrimeric G protein signaling via GIV/Girdin: breaking the rules of engagement, space, and time. Bioessays *38*, 379–393.

Aznar, N., Patel, A., Rohena, C.C., Dunkel, Y., Joosen, L.P., Taupin, V., Kufareva, I., Farquhar, M.G., and Ghosh, P. (2016b). AMP-activated protein kinase fortifies epithelial tight junctions during energetic stress via its effector GIV/Girdin. Elife *5*, e20795.

Baciu, P.C., Suleiman, E.A., Deryugina, E.I., and Strongin, A.Y. (2003). Membrane type-1 matrix metalloproteinase (MT1-MMP) processing of pro-alphav integrin regulates cross-talk between alphavbeta3 and alpha2beta1 integrins in breast carcinoma cells. Exp. Cell Res. *291*, 167–175.

Boehm, C., and Field, M.C. (2019). Evolution of late steps in exocytosis: conservation, specialization. Wellcome Open Res. *4*, 112.

Bos, P.D., Zhang, X.H., Nadal, C., Shu, W., Gomis, R.R., Nguyen, D.X., Minn, A.J., van de Vijver, M.J., Gerald, W.L., Foekens, J.A., and Massague, J. (2009). Genes that mediate breast cancer metastasis to the brain. Nature *459*, 1005–1009.

Boyd, C., Hughes, T., Pypaert, M., and Novick, P. (2004). Vesicles carry most exocyst subunits to exocytic sites marked by the remaining two subunits, Sec3p and Exo70p. J. Cell Biol. *167*, 889–901.

Brennwald, P., Kearns, B., Champion, K., Keranen, S., Bankaitis, V., and Novick, P. (1994). Sec9 is a SNAP-25-like component of a yeast SNARE complex that may be the effector of Sec4 function in exocytosis. Cell *79*, 245–258.

Camargo, L.M., Collura, V., Rain, J.C., Mizuguchi, K., Hermjakob, H., Kerrien, S., Bonnert, T.P., Whiting, P.J., and Brandon, N.J. (2007). Disrupted in Schizophrenia 1 Interactome: evidence for the close connectivity of risk genes and a potential synaptic basis for schizophrenia. Mol. Psychiatry *12*, 74–86.

Castagnino, A., Castro-Castro, A., Irondelle, M., Guichard, A., Lodillinsky, C., Fuhrmann, L., Vacher, S., Aguera-Gonzalez, S., Zagryazhskaya-Masson, A., Romao, M., et al. (2018). Coronin 1C promotes triple-negative breast cancer invasiveness through regulation of MT1-MMP traffic and invadopodia function. Oncogene *37*, 6425–6441.

Castro-Castro, A., Marchesin, V., Monteiro, P., Lodillinsky, C., Rosse, C., and Chavrier, P. (2016). Cellular and molecular mechanisms of MT1-MMP-dependent cancer cell invasion. Annu. Rev. Cell Dev. Biol. *32*, 555–576.

Chiang, S.H., Hou, J.C., Hwang, J., Pessin, J.E., and Saltiel, A.R. (2002). Cloning and functional characterization of related TC10 isoforms, a subfamily of Rho proteins involved in insulin-stimulated glucose transport. J. Biol. Chem. *277*, 13067–13073.

Coleman, B.D., Marivin, A., Parag-Sharma, K., Digiacomo, V., Kim, S., Pepper, J.S., Casler, J., Nguyen, L.T., Koelle, M.R., and Garcia-Marcos, M. (2016). Evolutionary conservation of a GPCR-independent mechanism of trimeric G protein activation. Mol. Biol. Evol. *33*, 820–837.

Cox, D.R. (1972). Regression models and life tables (with discussion). J. R. Statist. Soc. B *34*, 187–220.

Dalerba, P., Kalisky, T., Sahoo, D., Rajendran, P.S., Rothenberg, M.E., Leyrat, A.A., Sim, S., Okamoto, J., Johnston, D.M., Qian, D., et al. (2011). Single-cell dissection of transcriptional heterogeneity in human colon tumors. Nat. Biotechnol. *29*, 1120–1127.

Das, A., Monteiro, M., Barai, A., Kumar, S., and Sen, S. (2017). MMP proteolytic activity regulates cancer invasiveness by modulating integrins. Sci. Rep. *7*, 14219.

El Azzouzi, K., Wiesner, C., and Linder, S. (2016). Metalloproteinase MT1-MMP islets act as memory devices for podosome reemergence. J. Cell Biol. *213*, 109–125.

Enomoto, A., Murakami, H., Asai, N., Morone, N., Watanabe, T., Kawai, K., Murakumo, Y., Usukura, J., Kaibuchi, K., and Takahashi, M. (2005). Akt/PKB regulates actin organization and cell motility via Girdin/APE. Dev. Cell *9*, 389–402.

Finger, F.P., Hughes, T.E., and Novick, P. (1998). Sec3p is a spatial landmark for polarized secretion in budding yeast. Cell *92*, 559–571.

Galvez, B.G., Matias-Roman, S., Yanez-Mo, M., Sanchez-Madrid, F., and Arroyo, A.G. (2002). ECM regulates MT1-MMP localization with beta1 or alphavbeta3 integrins at distinct cell compartments modulating its internalization and activity on human endothelial cells. J. Cell Biol. *159*, 509–521.

Garcia-Marcos, M., Ghosh, P., and Farquhar, M.G. (2009). GIV is a nonreceptor GEF for G alpha i with a unique motif that regulates Akt signaling. Proc. Natl. Acad. Sci. U S A *106*, 3178–3183.

Ghosh, P. (2015). Heterotrimeric G proteins as emerging targets for network based therapy in cancer: end of a long futile campaign striking heads of a Hydra. Aging (Albany NY) *7*, 469–474.

Ghosh, P., Beas, A.O., Bornheimer, S.J., Garcia-Marcos, M., Forry, E.P., Johannson, C., Ear, J., Jung, B.H., Cabrera, B., Carethers, J.M., and Farquhar, M.G. (2010). A G{alpha}i-GIV molecular complex binds epidermal growth factor receptor and determines whether cells migrate or proliferate. Mol. Biol. Cell *21*, 2338–2354.

Ghosh, P., Rangamani, P., and Kufareva, I. (2017). The GAPs, GEFs, GDIs and...now, GEMs: new kids on the heterotrimeric G protein signaling block. Cell Cycle *16*, 607–612.

Gonzalo, P., Moreno, V., Galvez, B.G., and Arroyo, A.G. (2010). MT1-MMP and integrins: hand-to-hand in cell communication. Biofactors *36*, 248–254.

Guo, W., Grant, A., and Novick, P. (1999). Exo84p is an exocyst protein essential for secretion. J. Biol. Chem. *274*, 23558–23564.

Gupta, V., Bhandari, D., Leyme, A., Aznar, N., Midde, K.K., Lo, I.C., Ear, J., Niesman, I., Lopez-Sanchez, I., Blanco-Canosa, J.B., et al. (2016). GIV/Girdin activates Galphai and inhibits Galphas via the same motif. Proc. Natl. Acad. Sci. U S A *113*, E5721–E5730.

He, B., Xi, F., Zhang, X., Zhang, J., and Guo, W. (2007). Exo70 interacts with phospholipids and mediates the targeting of the exocyst to the plasma membrane. EMBO J. *26*, 4053–4065.

Hertzog, M., Monteiro, P., le Dez, G., and Chavrier, P. (2012). Exo70 subunit of the exocyst complex is involved in adhesion-dependent trafficking of caveolin-1. PLoS One *7*, e52627.

Hoshino, D., Branch, K.M., and Weaver, A.M. (2013). Signaling inputs to invadopodia and podosomes. J. Cell Sci. *126*, 2979–2989.

Howell, A.S., Jin, M., Wu, C.F., Zyla, T.R., Elston, T.C., and Lew, D.J. (2012). Negative feedback enhances robustness in the yeast polarity establishment circuit. Cell *149*, 322–333.

Hutagalung, A.H., Coleman, J., Pypaert, M., and Novick, P.J. (2009). An internal domain of Exo70p is required for actin-independent localization and mediates assembly of specific exocyst components. Mol. Biol. Cell *20*, 153–163.

Inoue, M., Chang, L., Hwang, J., Chiang, S.H., and Saltiel, A.R. (2003). The exocyst complex is required for targeting of Glut4 to the plasma membrane by insulin. Nature *422*, 629–633.

Jiang, P., Enomoto, A., Jijiwa, M., Kato, T., Hasegawa, T., Ishida, M., Sato, T., Asai, N., Murakumo, Y., and Takahashi, M. (2008). An actin-binding protein Girdin regulates the motility of breast cancer cells. Cancer Res. *68*, 1310–1318.

Juin, A., Billottet, C., Moreau, V., Destaing, O., Albiges-Rizo, C., Rosenbaum, J., Genot, E., and Saltel, F. (2012). Physiological type I collagen organization induces the formation of a novel class of linear invadosomes. Mol. Biol. Cell *23*, 297–309.

Kalogriopoulos, N.A., Rees, S.D., Ngo, T., Kopcho, N.J., Ilatovskiy, A.V., Sun, N., Komives, E.A., Chang, G., Ghosh, P., and Kufareva, I. (2019). Structural basis for GPCR-independent activation of heterotrimeric Gi proteins. Proc. Natl. Acad. Sci. U S A *116*, 16394–16403.

Ke, Y., Bao, T., Zhou, Q., Wang, Y., Ge, J., Fu, B., Wu, X., Tang, H., Shi, Z., Lei, X., et al. (2017). Discs large homolog 5 decreases formation and function of invadopodia in human hepatocellular carcinoma via Girdin and Tks5. Int. J. Cancer *141*, 364–376.

Leyme, A., Marivin, A., and Garcia-Marcos, M. (2016). GIV/Girdin (Galpha-interacting, vesicle-associated protein/girdin) creates a positive feedback loop that potentiates outside-in integrin signaling in cancer cells. J. Biol. Chem. *291*, 8269–8282.

Leyme, A., Marivin, A., Perez-Gutierrez, L., Nguyen, L.T., and Garcia-Marcos, M. (2015). Integrins activate trimeric G proteins via the nonreceptor protein GIV/Girdin. J. Cell Biol. *210*, 1165–1184.

Lin, C., Ear, J., Midde, K., Lopez-Sanchez, I., Aznar, N., Garcia-Marcos, M., Kufareva, I., Abagyan, R., and Ghosh, P. (2014). Structural basis for activation of trimeric Gi proteins by multiple growth factor receptors via GIV/Girdin. Mol. Biol. Cell *25*, 3654–3671.

Lin, C., Ear, J., Pavlova, Y., Mittal, Y., Kufareva, I., Ghassemian, M., Abagyan, R., Garcia-Marcos, M., and Ghosh, P. (2011). Tyrosine phosphorylation of the Galpha-interacting protein GIV promotes activation of phosphoinositide 3-kinase during cell migration. Sci. Signal. *4*, ra64.

Lin, W.H., Asmann, Y.W., and Anastasiadis, P.Z. (2015). Expression of polarity genes in human cancer. Cancer Inform. *14*, 15–28.

Liu, D., and Novick, P. (2014). Bem1p contributes to secretory pathway polarization through a direct interaction with Exo70p. J. Cell Biol. *207*, 59–72.

Liu, J., Yue, P., Artym, V.V., Mueller, S.C., and Guo, W. (2009). The role of the exocyst in matrix metalloproteinase secretion and actin dynamics during tumor cell invadopodia formation. Mol. Biol. Cell *20*, 3763–3771.

Lo, I.C., Gupta, V., Midde, K.K., Taupin, V., Lopez-Sanchez, I., Kufareva, I., Abagyan, R., Randazzo, P.A., Farquhar, M.G., and Ghosh, P. (2015). Activation of galphai at the golgi by GIV/girdin imposes finiteness in Arf1 signaling. Dev. Cell *33*, 189–203.

Lopez-Sanchez, I., Kalogriopoulos, N., LO, I.C., Kabir, F., Midde, K.K., Wang, H., and Ghosh, P. (2015a). Focal adhesions are foci for tyrosine-based signal transduction via GIV/Girdin and G proteins. Mol. Biol. Cell *26*, 4313–4324.

Lopez-Sanchez, I., Ma, G.S., Pedram, S., Kalogriopoulos, N., and Ghosh, P. (2015b). GIV/girdin binds exocyst subunit-Exo70 and regulates exocytosis of GLUT4 storage vesicles. Biochem. Biophys. Res. Commun. *468*, 287–293.

Lu, H., Liu, J., Liu, S., Zeng, J., Ding, D., Carstens, R.P., Cong, Y., Xu, X., and Guo, W. (2013). Exo70 isoform switching upon epithelial-mesenchymal transition mediates cancer cell invasion. Dev. Cell *27*, 560–573.

Ma, G., Lopez-Sanchez, I., Aznar, N., Kalogriopoulos, N., Midde, K., Ciaraldi, T.P., Henry, H.R., and Ghosh, P. (2015). Activation of G proteins by GIV-GEF is a pivot point for insulin resistance and sensitivity. Mol. Biol. Cell *26*, 4209–4223.

Martin-Urdiroz, M., Deeks, M.J., Horton, C.G., Dawe, H.R., and Jourdain, I. (2016). The exocyst complex in health and disease. Front. Cell Dev. Biol. *4*, 24.

Mccaffrey, L.M., and Macara, I.G. (2012). Signaling pathways in cell polarity. Cold Spring Harb. Perspect. Biol. *4*, a009654.

Mei, K., Li, Y., Wang, S., Shao, G., Wang, J., Ding, Y., Luo, G., Yue, P., Liu, J.J., Wang, X., et al. (2018). Cryo-EM structure of the exocyst complex. Nat. Struct. Mol. Biol. *25*, 139–146.

Midde, K., Sun, N., Rohena, C., Joosen, L., Dhillon, H., and Ghosh, P. (2018). Single-cell imaging of metastatic potential of cancer cells. iScience *10*, 53–65.

Minn, A.J., Gupta, G.P., Siegel, P.M., Bos, P.D., Shu, W., Giri, D.D., Viale, A., Olshen, A.B., Gerald, W.L., and Massague, J. (2005). Genes that mediate breast cancer metastasis to lung. Nature *436*, 518–524.

Mittal, Y., Pavlova, Y., Garcia-Marcos, M., and Ghosh, P. (2011). Src homology domain 2-containing protein-tyrosine phosphatase-1 (SHP-1) binds and dephosphorylates G(alpha)-interacting, vesicle-associated protein (GIV)/Girdin and attenuates the GIV-phosphatidylinositol 3-kinase (PI3K)-Akt signaling pathway. J. Biol. Chem. *286*, 32404–32415.

Monteiro, P., Rosse, C., Castro-Castro, A., Irondelle, M., Lagoutte, E., Paul-Gilloteaux, P., Desnos, C., Formstecher, E., Darchen, F., Perrais, D., et al. (2013). Endosomal WASH and exocyst complexes control exocytosis of MT1-MMP at invadopodia. J. Cell Biol. *203*, 1063–1079.

Moore, B.A., Robinson, H.H., and Xu, Z. (2007). The crystal structure of mouse Exo70 reveals unique features of the mammalian exocyst. J. Mol. Biol. *371*, 410–421.

Morton, W.M., Ayscough, K.R., and Mclaughlin, P.J. (2000). Latrunculin alters the actin-monomer subunit interface to prevent polymerization. Nat. Cell Biol. *2*, 376–378.

Nechiporuk, T., Fernandez, T.E., and Vasioukhin, V. (2007). Failure of epithelial tube maintenance

causes hydrocephalus and renal cysts in Dlg5-/- mice. Dev. Cell *13*, 338–350.

Nechipurenko, I.V., Olivier-Mason, A., Kazatskaya, A., Kennedy, J., Mclachlan, I.G., Heiman, M.G., Blacque, O.E., and Sengupta, P. (2016). A conserved role for girdin in basal body positioning and ciliogenesis. Dev. Cell *38*, 493–506.

Novick, P., Field, C., and Schekman, R. (1980). Identification of 23 complementation groups required for post-translational events in the yeast secretory pathway. Cell *21*, 205–215.

Ohara, K., Enomoto, A., Kato, T., Hashimoto, T., Isotani-Sakakibara, M., Asai, N., Ishida-Takagishi, M., Weng, L., Nakayama, M., Watanabe, T., et al. (2012). Involvement of Girdin in the determination of cell polarity during cell migration. PLoS One *7*, e36681.

Picco, A., Irastorza-Azcarate, I., Specht, T., Boke, D., Pazos, I., Rivier-Cordey, A.S., Devos, D.P., Kaksonen, M., and Gallego, O. (2017). The in vivo architecture of the exocyst provides structural basis for exocytosis. Cell *168*, 400–412.e18.

Planchon, D., Rios Morris, E., Genest, M., Comunale, F., Vacher, S., Bieche, I., Denisov, E.V., Tashireva, L.A., Perelmuter, V.M., Linder, S., et al. (2018). MT1-MMP targeting to endolysosomes is mediated by upregulation of flotillins. J. Cell Sci. *131*, jcs218925.

Puseenam, A., Yoshioka, Y., Nagai, R., Hashimoto, R., Suyari, O., Itoh, M., Enomoto, A., Takahashi, M., and Yamaguchi, M. (2009). A novel Drosophila Girdin-like protein is involved in Akt pathway control of cell size. Exp. Cell Res. *315*, 3370–3380.

Rahman-Zaman, A., Shan, S., and Reinhart-King, C.A. (2018). Cell migration in microfabricated 3D collagen microtracks is mediated through the prometastatic protein girdin. Cell Mol. Bioeng. *11*, 1–10.

Sahoo, D., Dill, D.L., Tibshirani, R., and Plevritis, S.K. (2007). Extracting binary signals from microarray time-course data. Nucleic Acids Res. *35*, 3705–3712.

Sasaki, K., Kakuwa, T., Akimoto, K., Koga, H., and Ohno, S. (2015). Regulation of epithelial cell polarity by PAR-3 depends on Girdin transcription and Girdin-Galphai3 signaling. J. Cell Sci. *128*, 2244–2258.

Shi, F., and Sottile, J. (2011). MT1-MMP regulates the turnover and endocytosis of extracellular matrix fibronectin. J. Cell Sci. *124*, 4039–4050.

Stahelin, R.V., Karathanassis, D., Murray, D., Williams, R.L., and Cho, W. (2007). Structural and membrane binding analysis of the Phox homology domain of Bem1p: basis of phosphatidylinositol 4-phosphate specificity. J. Biol. Chem. *282*, 25737–25747.

Steffen, A., Le Dez, G., Poincloux, R., Recchi, C., Nassoy, P., rottner, K., Galli, T., and Chavrier, P. (2008). MT1-MMP-dependent invasion is regulated by TI-VAMP/VAMP7. Curr. Biol. *18*, 926–931.

Suzuki, A., and Ohno, S. (2006). The PAR-aPKC system: lessons in polarity. J. Cell Sci. *119*, 979–987.

Terbush, D.R., Maurice, T., Roth, D., and Novick, P. (1996). The Exocyst is a multiprotein complex required for exocytosis in Saccharomyces cerevisiae. EMBO J. *15*, 6483–6494.

Terbush, D.R., and Novick, P. (1995). Sec6, Sec8, and Sec15 are components of a multisubunit complex which localizes to small bud tips in Saccharomyces cerevisiae. J. Cell Biol. *130*, 299–312.

Thompson, B.J. (2013). Cell polarity: models and mechanisms from yeast, worms and flies. Development *140*, 13–21.

Volkmer, J.P., Sahoo, D., Chin, R.K., Ho, P.L., Tang, C., Kurtova, A.V., Willingham, S.B., Pazhanisamy, S.K., Contreras-Trujillo, H., Storm, T.A., et al. (2012). Three differentiation states risk-stratify bladder cancer into distinct subtypes. Proc. Natl. Acad. Sci. U S A *109*, 2078–2083.

Wang, S.H., Celic, I., Choi, S.Y., Riccomagno, M., Wang, Q., Sun, L.O., Mitchell, S.P., Vasioukhin, V., Huganir, R.L., and Kolodkin, A.L. (2014). Dlg5 regulates dendritic spine formation and synaptogenesis by controlling subcellular N-cadherin localization. J. Neurosci. *34*, 12745–12761.

Wang, Y., Klijn, J.G., Zhang, Y., Sieuwerts, A.M., Look, M.P., Yang, F., Talantov, D., Timmermans, M., Meijer-van Gelder, M.E., Yu, J., et al. (2005). Gene-expression profiles to predict distant metastasis of lymph-node-negative primary breast cancer. Lancet *365*, 671–679.

Wu, B., and Guo, W. (2015). The exocyst at a glance. J. Cell Sci. *128*, 2957–2964.

Yeaman, C., Grindstaff, K.K., and Nelson, W.J. (2004). Mechanism of recruiting Sec6/8 (exocyst) complex to the apical junctional complex during polarization of epithelial cells. J. Cell Sci. *117*, 559–570.

Zhang, X., Orlando, K., He, B., Xi, F., Zhang, J., Zajac, A., and Guo, W. (2008). Membrane association and functional regulation of Sec3 by phospholipids and Cdc42. J. Cell Biol. *180*, 145–158.

Zhao, Y., Liu, J., Yang, C., Capraro, B.R., Baumgart, T., Bradley, R.P., Ramakrishnan, N., XU, X., Radhakrishnan, R., Svitkina, T., and Guo, W. (2013). Exo70 generates membrane curvature for morphogenesis and cell migration. Dev. Cell *26*, 266–278.

Zigrino, P., Drescher, C., and Mauch, C. (2001). Collagen-induced proMMP-2 activation by MT1-MMP in human dermal fibroblasts and the possible role of alpha2beta1 integrins. Eur. J. Cell Biol. *80*, 68–77.

Zuo, X., Zhang, J., Zhang, Y., Hsu, S.C., Zhou, D., and Guo, W. (2006). Exo70 interacts with the Arp2/3 complex and regulates cell migration. Nat. Cell Biol. *8*, 1383–1388.

iScience, Volume *23*

Supplemental Information

GIV/Girdin and Exo70 Collaboratively Regulate the Mammalian Polarized Exocytic Machinery

Cristina Rohena, Navin Rajapakse, I-Chung Lo, Peter Novick, Debashis Sahoo, and Pradipta Ghosh

SUPPLEMENTAL ONLINE MATERIALS

INVENTORY OF SUPPLEMENTARY MATERIALS

- **STAR METHODS**
- **SUPPLEMENTARY FIGURES AND LEGENDS**
- **REFERENCES CITED**

TRANSPARENT METHODS

- **KEY RESOURCE TABLE**
- **CONTACT FOR REAGENT AND RESOURCE SHARING**
- **EXPERIMENTAL MODEL AND SUBJECT DETAILS**
    - Cell Lines (Cos7, MDA-MB-231)
- **METHOD DETAILS**
    - Plasmid constructs
    - Protein Expression and Purification
    - Cell culture, transfection, lysis, and quantitative immunoblotting
    - Whole Cell Immunofluorescence and TIRF microscopy
    - Generation of stable cell lines
    - In Vitro Pulldown and Co-immunoprecipitation (Co-IP)
    - Gelatin Degradation Assay
    - Adhesion Assay
    - Transwell Invasion Assay
    - Analysis of gene expression data
- **QUANTIFICATION AND STATISTICAL ANALYSIS**
    - Statistical Analysis
    - Replications
- **DATA AND SOFTWARE AVAILABILITY**

Key Resource Table:

REAGENT or RESOURCE	SOURCE	IDENTIFIER
Antibodies and fluorophores		
Rabbit monoclonal anti-pY1765 GIV	Roche Spring Biosciences	06974937001 Clone SP158
Rabbit polyclonal anti-GIV CT	Santa Cruz Biotechnology	N/A
Rabbit polyclonal anti-Gαi3 (C-10)	Santa Cruz Biotechnology	N/A
Rabbit polyclonal anti-β-tubulin	Santa Cruz Biotechnology	sc-9104
Mouse monoclonal anti-GAPDH	Santa Cruz Biotechnology	sc-365062
Mouse monoclonal anti-HIS	GenScript	A00186-100
Mouse monoclonal anti-GST	GenScript	A00865
Mouse monoclonal anti-HA		
Rabbit monoclonal anti-cortactin	Santa Cruz Biotechnology	N/A
Goat anti-Rabbit IgG (680)	LI-COR Biosciences	926-68071
Goat anti-Rabbit IgG, Alexa Fluor 594 conjugated	ThermoFisher Scientific	A11072
Goat anti-Rabbit IgG, Alexa Fluor 647 conjugated	ThermoFisher Scientific	A27040
Goat anti-Mouse IgG (800)	LI-COR Biosciences	926-32210
Goat anti-Mouse IgG, Alexa Fluor 488 conjugated	Thermo Fisher Scientific	A11017
Biological Samples and Cell Lines		
Cos7	ATCC	CRL-1651
MDA-MB-231	ATCC	HTB-26
Chemicals, Recombinant Proteins, and Plasmids		
DAPI (4',6-Diamidino-2-Phenylindole, Dilactate)	Thermo Fisher Scientific	D3571
Collagen I	BD Biosciences	354249
Poly-D-lysine	Millipore Sigma	A-003-E
Mirus TranIT LT1	Mirus Bio LLC	MIR2300
G418	Cellgro	A-1720
Puromycin	Life Technologies	A1113803
Porcine Gelatin		
Paraformaldehyde 16%	Electron Microscopy Biosciences	15710
Phalloidin 594	Thermo Fisher Scientific	A12381
Prolong Gold	Thermo Fisher Scientific	P10144
Prolong Glass	Thermo Fisher Scientific	P36980
GST- Exo70 (human)	*Xiong X. et al., Mol Biol Cell., 2012.* *--Kun Ling*	N/A
Exo-70-HA (human)	*Sakurai-Yageta et al., 2008.* *--Phillipe Chavrier*	N/A
pGEX-4T-GIV-CT-WT (a.a. 1623-1870)	*Garcia-Marcos et al., 2009*	N/A
pET-28b-GIV-CT-WT (a.a. 1660-1870)	*Garcia-Marcos et al., 2009*	N/A
pET-28b-GIV-CT-PGxA (a.a. 1660-1870)	This paper	N/A
pET-28b-GIV-CT-AAxA (a.a. 1660-1870)	This paper	
pET-28b-GIV-CT-PAxF (a.a. 1660-1870)	This paper	
pET-28b-GIV-CT-AAxF (a.a. 1660-1870)	This paper	
pET-28b-GIV-CT-PGRF (a.a. 1660-1870)	This paper	
pET-28b-GIV-CT-DFYR (a.a. 1660-1870)	This paper	
pET-28b-GIV-CT-AFYD (a.a. 1660-1870)	This paper	
pET-28b-GIV-CT-DFYA (a.a. 1660-1870)	This paper	
pET-28b-GIV-CT-DFAD (a.a. 1660-1870)	This paper	
pET-28b-GIV-CT-AFYA (a.a. 1660-1870)	This paper	
pET-28b-GIV-CT-DFYDL (a.a. 1660-1870)	*Lin et. al, MBoC 2014*	
CMV14-p3X FLAG-GIV WT (full length)	This paper	N/A
CMV14-p3X FLAG-GIV P1742A (full length)	This paper	N/A
CMV14-p3X FLAG-GIV AAxA (full length)	This paper	N/A
pGEX4T2-Exo70p full length	*Liu and Novick, JCB 2014* *--Peter Novick*	N/A
pGEX4T2-Exo70p Δ62N (Exo70Δ1-62)	*Liu and Novick, JCB 2014*	N/A
pGEX4T2-Exo70p Δ dA (Exo70 Δ 1-140)	*Liu and Novick, JCB 2014* *--Peter Novick*	N/A
pGEX4T2-Exo70p Δ dB (Exo70 Δ 153-302)	*Liu and Novick, JCB 2014* *--Peter Novick*	N/A
pGEX4T2-Exo70p Δ dAB (Exo70 Δ 1-338)	*Liu and Novick, JCB 2014* *--Peter Novick*	N/A
pGEX4T2-Exo70p Δ dC (Exo70 Δ 347-514)	*Liu and Novick, JCB 2014*	N/A

	--Peter Novick	
pGEX4T2-Exo70p Δ dD (Exo70 Δ 542-623)	*Liu and Novick, JCB 2014* *--Peter Novick*	N/A
pGEX4T2-Exo70p, M26 (pGEX4T2Exo70S196F/L246S/K354A/K355A/E488A/K489A/E505A/R506A)	*Liu and Novick, JCB 2014* *--Peter Novick*	
pGEX4T2-Exo70p, M30 (pGEX4T2-Exo70L246S/K354A/K355A/E488A/K489A/E505A/R506A)	*Liu and Novick, JCB 2014* *--Peter Novick*	
pGEX4T2-Bem1	*Liu and Novick, JCB 2014* *--Peter Novick*	
pET21a-Bem1	*Liu and Novick, JCB 2014* *--Peter Novick*	
MT1-MMP–mCherry	*Sakurai-Yageta et al, JCB 2008* *--Phillipe Chavrier*	
MT1-MMP-pHLuorin	*Lizarraga et al Cancer Res. 2009 – Phillipe Chavrier*	
Software		
ImageJ	National Institute of Health	https://imagej.net/Welcome
Prism	GraphPad	https://www.graphpad.com/scientific-software/prism/
LAS-X	Leica	www.leica-microsystems.com/products/microscope-software/p/leica-las-x-ls

Methods

Plasmid constructs

Cloning of GIV-CT (aa 1660–1870) into pET28b (His-GIV CT) and GIV-CT (aa 1623-1870) were described previously (Garcia-Marcos et al., 2012). pGEX4T2Exo70p, pGEX4T2-Exo70Δ62N (Exo70Δ1-62), pGEX4T2-Exo70 Δ dA (Exo70 Δ 1-140), pGEX4T2-Exo70 Δ dB (Exo70 Δ 153-302), pGEX4T2-Exo70 Δ dAB (Exo70 Δ 1-338), pGEX4T2-Exo70 Δ dC (Exo70 Δ 347-514), pGEX4T2-Exo70 Δ dD (Exo70 Δ 542-623), pGEX4T2-Exo70M26, pGEX4T2-Exo70M30, pGEX4T2-Bem1, and pET21a-Bem1 plasmids were generously obtained from Peter Novick (UCSD, California). MT1-MMP–mCherry and MT1-MMP-pHLuorin plasmids were generously shared by Phillipe Chavrier. For mammalian expression, RNA interference–resistant (shRNA rest) GIV was cloned into p3XFLAG-CMVTM-14 plasmid (GIV-FLAG) as described previously (Garcia-Marcos et al., 2009). GIV-FLAG and His-GIV-CT mutants (detailed in table) were generated by site-directed mutagenesis using a QuikChange kit (Stratagene) and specific primers (sequence available upon request) as per the manufacturer's protocols (Garcia-Marcos et al., 2009, Lin et al., 2011). Primer sequences are available upon request. shRNA 3–untranslated region for GIV (GIV shRNA:CCGGGCTTTCATT-ACCAGCTCTGAACTCGAGTTCAGAGCTGGTAATGAAAGCTTTTTTG) was cloned into pLKO.1 (TRCN0000130452) or control vector TRC1.5-pLKO.1-puro. GST-Exo70 (Xiong et al., 2012) was obtained from Kun Ling (Mayo Clinic). Exo70-HA (Sakurai-Yageta et al., 2008) was obtained from Philippe Chavrier (Institut Curie, France).

Protein expression and purification

Both GST and His-tagged proteins were expressed in E. coli stain BL21 (DE3) and purified as previously described (Garcia-Marcos et al., 2009, Ghosh et al., 2008). Briefly, cultures were induced using 1 mM IPTG overnight at 25°C. Cells were then pelleted and resuspended in either GST lysis buffer (25 mM Tris-HCl, pH 7.5, 20 mM NaCl, 1 mM EDTA, 20% (vol/vol) glycerol, 1% (vol/vol) Triton X-100, 2×protease inhibitor cocktail) or His lysis buffer (50 mM NaH_2PO_4 (pH 7.4), 300 mM NaCl, 10 mM imidazole, 1% (vol/vol) Triton X-100, 2X protease inhibitor cocktail). Cells were lysed by sonication, and lysates were cleared by centrifugation at 12,000 X g at 4°C for 30 mins. Supernatant was then affinity purified using glutathione-Sepharose 4B beads (GE Healthcare) or HisPur Cobalt Resin (Thermo Fisher Scientific), followed by elution, overnight dialysis in PBS, and then storage at -80°C.

His-GIV-CT fusion construct was expressed in E. coli strain BL21 (DE3) and purified as described previously. Briefly, bacterial cultures were induced overnight at 25°C with 1 mM isopropyl β-d-1-thiogalactopyranoside (IPTG). Pelleted bacteria from 1 l of culture were resuspended in 10 ml of His lysis buffer (50 mM NaH2PO4, pH 7.4, 300 mM NaCl, 10 mM imidazole, 1% [vol:vol] Triton X-100, 2X protease inhibitor cocktail [Complete EDTA-free, Roche Diagnostics, CA, USA]). After sonication (3 × 30 s), lysates were centrifuged at 12,000 × g at 4°C for 20 min. Solubilized proteins were affinity purified on HisPur Cobalt Resin (Pierce, IL, USA). Proteins were eluted, dialyzed overnight against PBS, and stored at −80°C.

Cell culture, transfection, lysis, and quantitative immunoblotting

Unless mentioned otherwise, cell lines used in this work were cultured according to American Type Culture Collection (ATCC) guidelines or guidelines previously published for each line Cos7, HeLa and MDA-MB-231 cells were obtained from American Type Culture Collection (ATCC). Transfection, lysis, and immunoblotting were carried out exactly as described before (Aznar et al., 2016, Lopez-Sanchez et al., 2015) Cells were transfected using Mirus LT1 following the manufacturers' protocols. For assays involving serum starvation, serum concentration was reduced to 0% FBS overnight.

Whole-cell lysates were prepared after washing cells with cold PBS before resuspending and boiling them in sample buffer. Lysates used as a source of proteins in pull-down assays were prepared by resuspending cells in lysis buffer (20 mM HEPES, pH 7.2, 5 mM Mg acetate, 125 mM K acetate, 0.4% Triton X-100, and 1 mM dithiothreitol supplemented with sodium orthovanadate [500 μM], phosphatase [Sigma-Aldrich, MO, USA], and protease [Roche, USA] inhibitor cocktails), after which they were passed through a 28-gauge needle at 4°C and cleared (10,000 × g for 10 min) before use in subsequent experiments.

For immunoblotting, protein samples were separated by SDS-PAGE and transferred to polyvinylidene fluoride membranes (Millipore Sigma, MO, USA). Membranes were blocked with PBS supplemented with 5% nonfat milk (or with 5% BSA when probing for phosphorylated proteins) before incubation with primary antibodies. In some instances, the samples were separated on a 12% SDS PAGE and transferred to a nitrocellulose membrane (Bio-Rad, CA, USA) using TransBlot-Turbo (Bio-Rad, CA, USA). The membrane was stained with Ponceau S to visualize baits, then washed and blocked with PBS with 0.1% Tween (PBS-T) and 0.5% BSA overnight at 4°C. Infrared imaging with two-color detection and quantification were performed using a

Li-Cor Odyssey imaging system. Dilution of primary antibodies used were as follows: anti–GIV-CT, 1:500; anti-Gαi3, 1:333; anti-β tubulin, 1:1000; and anti–His, 1:500. All blots were visualized using LI-COR Odyssey imager, and band analysis was performed with Image Studio™ Lite 5.2 (LI-COR Biosciences, NE, USA). Figures were assembled for presentation using Photoshop (Adobe, San Jose, CA, USA) and Illustrator (Adobe, San Jose, CA, USA) software.

In Vitro Pulldown and Co-immunoprecipitation (Co-IP)

Purified GST-tagged proteins from E. coli were immobilized onto glutathione-Sepharose beads and incubated with binding buffer (50 mM Tris-HCl pH 7.4, 100 mM NaCl, 0.4% (v:v) Nonidet P-40, 10 mM MgCl2, 5 mM EDTA, 2 mM DTT, 1X Complete protease inhibitor) for 60min at room temperature. For GST-pulldown assays with recombinant proteins, the proteins were diluted in binding buffer and incubated with immobilized GST-proteins for 90min at room temperature. For binding with cell lysates, cells were lysed in cell lysis buffer (20 mM HEPES pH 7.2, 5 mM Mg-acetate, 125 mM K-acetate, 0.4% Triton X-100, 1 mM DTT, 500 μM sodium orthovanadate, phosphatase inhibitor cocktail (Sigma-Aldrich, MO, USA) and protease inhibitor cocktail (Roche Life Science)) using a 28G syringe, followed by centrifugation at 10,000Xg for 10min. Cleared supernatant was then used in binding reaction with immobilized GST-proteins for 4 hours at 4°C. After binding, bound complexes were washed four times with 1 ml phosphate wash buffer (4.3 mM Na2HPO4, 1.4 mM KH2PO4, pH 7.4, 137 mM NaCl, 2.7 mM KCl, 0.1% (v:v) Tween 20, 10 mM MgCl2, 5 mM EDTA, 2 mM DTT, 0.5 mM sodium orthovanadate). Bound proteins were then eluted through boiling at 100°C in Laemmli buffer (BIORAD, CA, USA).

Whole-cell immunofluorescence

Cells were fixed at room temperature with 3% PFA in PBS for 15 min, treated with 0.1 M glycine for 10 min, and subsequently permeabilized for 1 h (0.2% Triton X-100 in PBS) and blocked in PBS containing 1% bovine serum albumin (BSA) and 0.1% Triton X-100 as described previously (Lopez-Sanchez et al., 2014 blue right-pointing triangle). Primary and secondary antibodies where incubated for 1 h at room temperature in blocking buffer. ProLong Gold or Prolong Glass (Life Technologies) was used as mounting medium. Dilutions of antibodies and/or fluorophores used were as follows: HA, 1:500; phalloidin, 1:1000; cortactin, 1:500; DAPI, 1:2000; and secondary goat anti-rabbit (488), goat anti-mouse (594), and goat-anti-mouse or rabbit (647) Alexa-conjugated antibodies, 1:500. Images were acquired at room temperature with a Leica TCS SP8 with DMI8 microscope equipped with a PMT and HyD detectors and the LAS X (Leica) software using a 100× oil-immersion objective using a white light laser tunable to 488-, 561-, 635-, and 405-nm for excitation. The settings were optimized, and the final images scanned with line averaging of three scans. Images were further processed using Lightning deconvolution in the Leica LAS-X software package. All images were processed using ImageJ software and assembled for presentation using Photoshop and Illustrator software (Adobe, San Jose, CA). Images shown are representative of 90–95% cells that were evaluated across three independent experiments.

Cells were plated on gelatin-coated coverslips and allowed to adhere for 30 min. They were then fixed with 4% PFA and stained with antibodies against cortactin (1:100), HA (1:100) or direct fluorescence from MT1-MMP mCherry construct followed by secondary antibody incubation (AlexaFluor 488 and AlexaFluor 647 1:500).

Coverslips were then mounted on Prolong Glass and allowed to cure for 5 days before imaging. Once images were acquired, they were deconvolved using LAS-X software and then processed using Image-J. All images were further processed in Image-J using the 3D surface plot plugin and line scans were done to generate RGB plots. We also carried out colocalization analyses using the Pearson's correlation coefficient, which was measured from each split channel after background subtraction. Fluorescence background was subtracted from a 2x2 pixel region outside the cells using the "ROI background subtraction" plugin of the ImageJ software. Two standard deviations of background from mean fluorescence intensity were typically subtracted.

Generation of stable cell lines

ShRNA control and shRNA GIV MDA-MB-231, stable cell lines using Mission RNAi technology (Sigma-Aldrich, MO, USA) were generated by lentiviral transduction followed by selection with puromycin (2.5 µg/ml) a described previously (Midde et al., 2018). Depletion of endogenous GIV was confirmed by immunoblotting with GIV-CT rabbit antibody. Lentiviral packaging was performed in HEK293T cells by co-transfecting the shRNA constructs with psPAX2 and pMD2G plasmids (4:3:1 ratio, respectively), using Mirus LT1. The medium was changed after 24 h, and virus-containing medium was collected after 36–48 h and centrifuged and filtered through a 0.45-µm filter. psPAX2 and pMD2G plasmids were a generous gift from Christopher K. Glass (University of California, San Diego, La Jolla, CA). shRNA GIV MDA-MB-231 stable cell lines expressing p3xFLAG-CMV-14-GIV (GIV-3xFLAG) WT, GIV-PGxA and AAxA constructs were selected as previously described (Aznar et al., 2016) with the neomycin analogue G418 at 800 µg/ml. Expression of various GIV constructs were confirmed to be similar to levels of endogenous GIV in shRNA control cells by immuno-blotting with GIV-CT antibodies.

Fluorescent gelatin degradation assay

MDA-MB-231 cells were incubated for 5 h on FITC-conjugated cross-linked gelatin, and then fixed and stained for F-actin. Cells were imaged with the 63× objective of a Leica TCS SPE confocal microscope and controlled by LAS software. For quantification of degradation, the total area of degraded matrix in one field (black pixels) measured with the Threshold command of ImageJ was divided by the number of phalloidin-labeled cells in the field to define a degradation index, which was normalized to the degradation index of control cells set to 100. All experiments were performed in triplicate, and each experiment was repeated at least three times.

Total internal reflection of fluorescence (TIRF)- Microscopy

MDA-MB-231 cells transfected with pHLuorin-tagged MT1-MMP were plated on glass-bottom dishes coated with cross-linked unlabeled gelatin as previously described. TIRFM sequences were acquired on an inverted microscope (TE2000) equipped with a 100× TIRF objective (1.47 NA), a TIRF arm, an image splitter (DV; Roper Scientific) installed in front of the CCD camera and a temperature controller. pHLuorin was excited with 491-laser, (100 mW; Roper Scientific), both controlled for power by an acousto-optic tunable filter. Fluorescent emissions were selected with bandpass and longpass filters (Chroma Technology Corp.) and captured by a QuantEM EMCCD camera (Roper Scientific). To measure the sub-plasma membrane density of MT1-MMP endosomes, cells stably expressing MT1-MMP-pHLuorin were plated on a layer of unlabeled gelatin and imaged

by TIRFM for an exposure time of 100 ms and with 1 pixel corresponding to 160 nm. The density of MT1-MMP-pHLuorin structures was evaluated by ImageJ and quantified using the particle analyzer application on ImageJ (National Institutes of Health, Bethesda, MD) exactly as outlined previously (Horzum et al., 2014). The threshold was set at 1.3× the cytoplasmic background.

Transwell invasion assay

Cell invasion was assessed using Biocoat Matrigel (Corning, NY, USA) inserts with 8-μm pores in 24-well plates. Cells were detached using trypsin/EDTA and resuspended in DMEM supplemented with 0.4% FBS. A total of 5 × 10^5 cells was loaded in the upper well in a volume of 300 μl, and the lower well was filled with 750 μl of DMEM with 10% FBS. The plates were incubated at 37°C for 24h before removing the remaining cell suspension. The invasion insert was placed in a clean well containing 4% PFA for 1 h at room temperature, stained with crystal violet for 1 h, and washed three times in PBS. Cells on the upper side of the filters were removed with cotton-tipped swabs, and the number of migrated cells on the bottom side of the filter was counted in five randomly chosen fields at 200× magnification and averaged. All experiments were performed in triplicate, and each experiment was repeated at least three times.

Adhesion Assay

12-well plates were coated with collagen, rinsed with PBS, and then blocked with 0.5% BSA for 1h at 37°C. Cells were harvested with trypsin/EDTA, seeded in the wells at 2 × 104 cells/well in 1,000 μl of DMEM with 0.4% FBS, and allowed to adhere for 30min at 37°C. Nonadherent cells were removed by gentle washing twice with PBS, and attached cells were fixed in 4% PFA for 15 min and then stained with 2.3% crystal violet (Sigma-Aldrich, MO, USA) for 10min. Cells were extensively washed, air dried, and then the cells imaged and counted using ImageJ. All experiments were performed in triplicate, and each experiment was repeated at least three times.

Analysis of gene expression data

Gene expression data from three different cohorts of patients with breast cancers (Minn et al., 2005, Bos et al., 2009, Wang et al., 2005) were collected from the National Center for Biotechnology Information (NCBI) Gene Expression Omnibus (GEO) website (Barrett, T. et al. 2005; Edgar et al., 2002). The dataset was prepared by pooling data from GSE2034, GSE2603 and GSE12276 and normalizing them together using Robust Multi-chip Average (RMA) algorithm. Patient survival data were carefully annotated for Kaplan-Meier analysis. To derive optimal cut-off values of gene expression levels, they are ordered from low to high and a rising step function was computed to define a threshold by StepMiner algorithm (Sahoo et al., 2007). Gene expression values were converted to high and low levels based on the StepMiner threshold. A noise margin of +/- 0.5 was used around the StepMiner threshold to provide relaxed estimates of the high/low values. A noise margin of +/- 0.5 around StepMiner threshold was used to soften or harden the actual threshold. Time-dependent survival probabilities are estimated with the Kaplan-Meier method (Kaplan EL, 1958) and compared using the log-rank test (Peto et al., 1977). Cox proportional-hazards regression models and life-tables (Cox, 1972) were used to test the

statistical interaction between two different genes based on their association with survival outcome. High and low expression patterns for focal genes such as GIV (CCDC88A), Exo70 (EXOC7) and Dlg5 (DLG5) were compared individually using Kaplan-Meier analyses in R statistical software (R version 3.4.4 2018-03-15). Statistical interaction (synergistic effects) between polarity determinant genes (Lin et al., 2015) and Exo70 (EXOC7) were measured using interaction terms in Cox proportional hazards regression model on the above pooled breast cancer dataset with survival data. For example, coefficient of interaction terms was computed from Cox regression model for CCDC88A and EXOC7 as follows:

$$\mathrm{h(t)} = \mathrm{h_0(t)exp(a1 * CCDC88A + a2 * EXOC7 + a3 * CCDC88A * EXOC7)}$$

where $\mathrm{h(t)}$ is the hazard rate at time t for an individual; $\mathrm{a1, a2, and\ a3}$ are the regression coefficients; $\mathrm{h_0(t)}$ is the baseline hazard; two indicator variables $\mathrm{CCDC88A}$ and $\mathrm{EXOC7}$ (high expression = 1 else 0) that had only additive or interactive effects; $\mathrm{a3}$ is the coefficient of interaction terms.

Data analysis and other methods

All experiments were repeated at least three times, and results were presented either as one representative experiment or as average ± S.E.M. Statistical significance was assessed with the Student's t test. Statistical significance between datasets with three or more experimental groups was determined using one-way analysis of variance (ANOVA) including a Tukey's test for multiple comparisons. For all tests, a p-value of 0.05 was used as the cutoff to determine significance [*p < 0.05, **p < 0.01, ***p < 0.001, ****p < 0.0001]. All experiments were repeated a least three times, and p-values are indicated in each figure. All statistical analysis was performed using GraphPad prism 8.

Data and resource sharing

All data and constructs are available for sharing.

SUPPLEMENTARY FIGURES AND LEGENDS

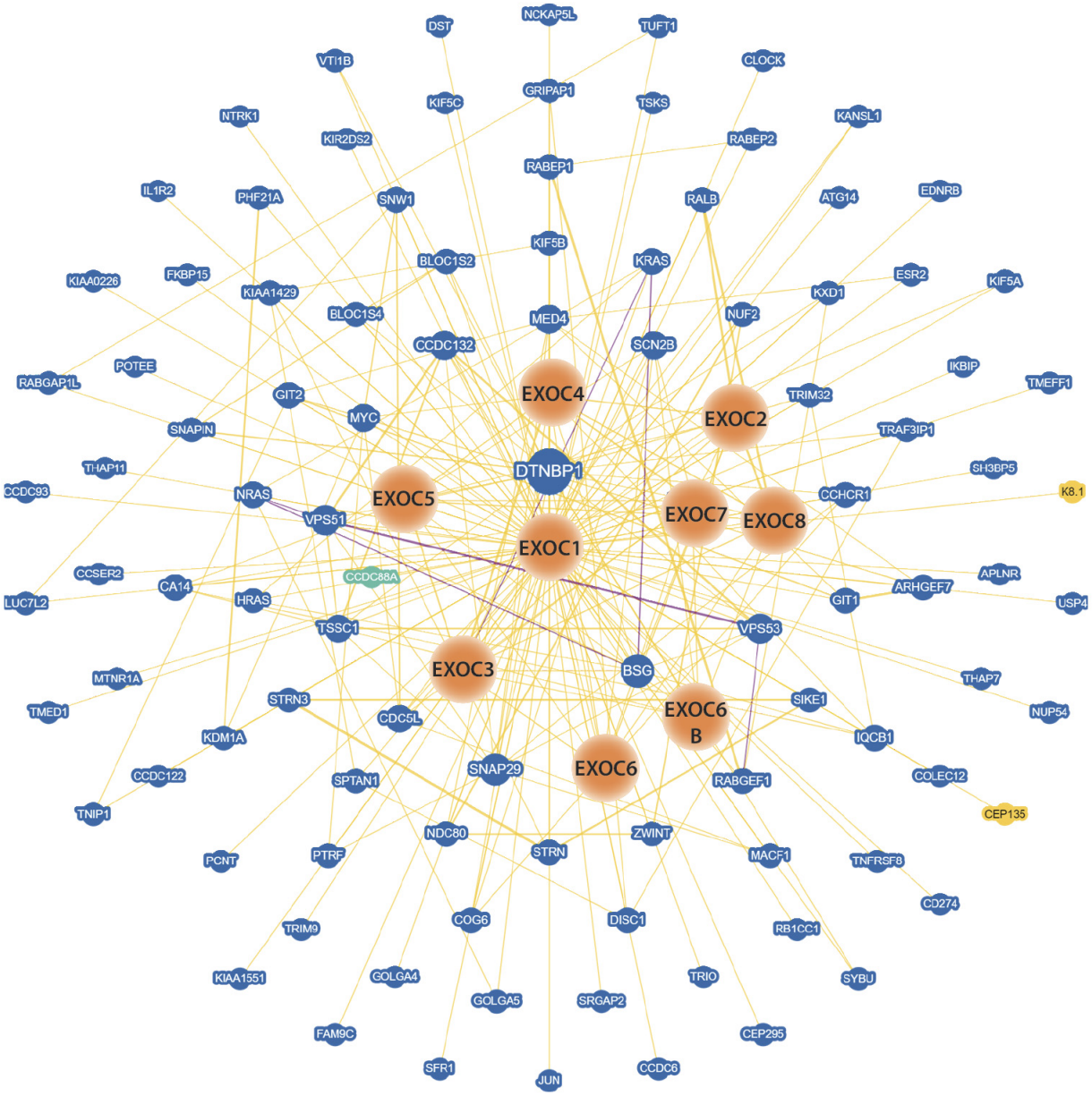

Supplementary Figure 1 [related to Figure 1]

The exocyst interactome includes the polarity scaffold GIV/Girdin. Visualization of the physical associations the subunits of the exocyst complexes using BioGRID (Version 3.5.178). CCDC88A (GIV/Girdin) is highlighted in green. Exocyst complex subunits are highlighted in orange. Blue nodes = associated protein from same species; yellow nodes = associated protein from another organism.

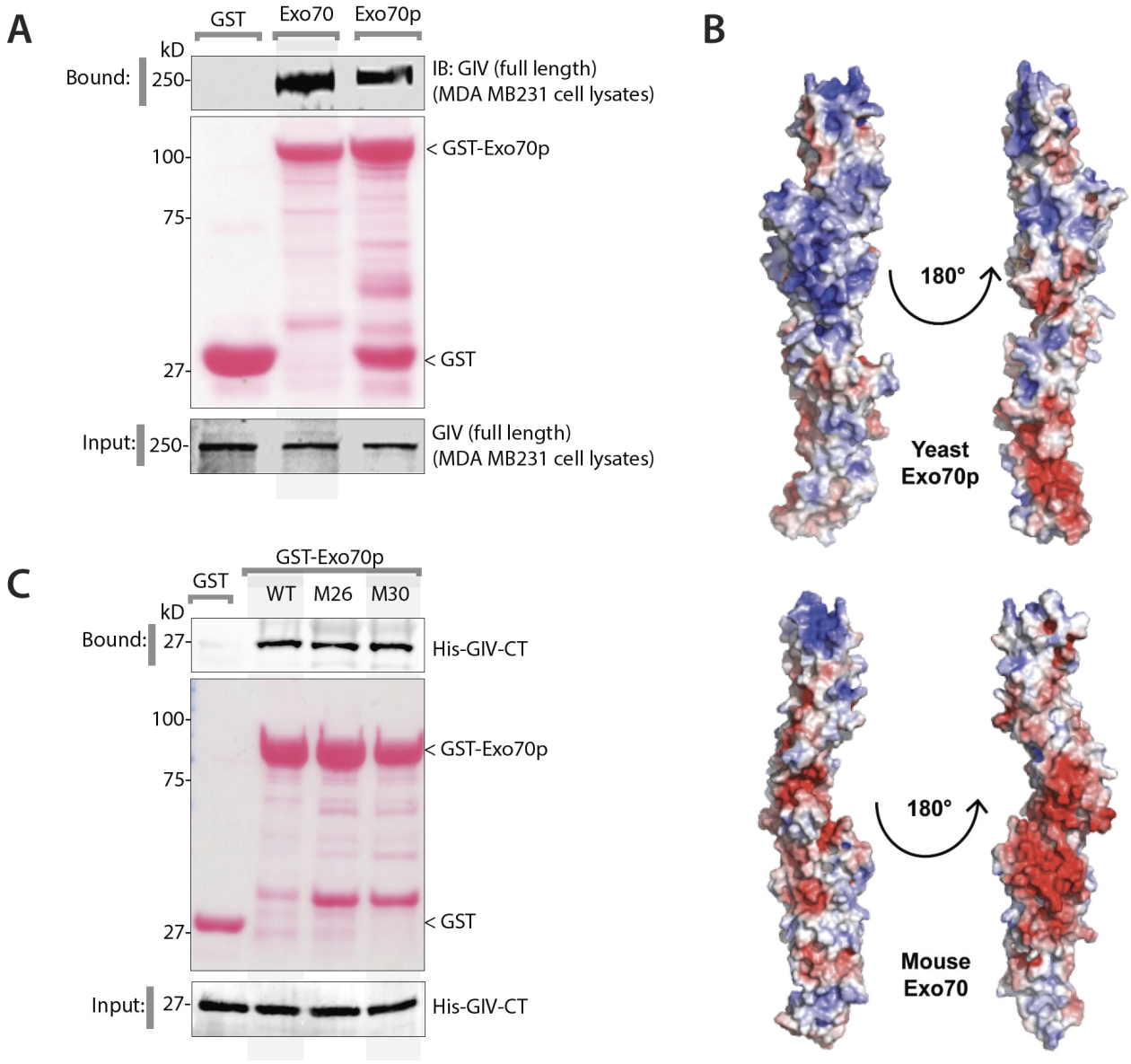

Supplementary Figure 2 [related to Figure 1]

GIV binds Exo70 similar to Bem1p but contact residues on Exo70 differ.

(A) Equal aliquots of lysates of MDA-MB-231 cells were used as source for full-length endogenous GIV in GST pulldown assays with GST, GST-Exo70p and GST-Exo70 proteins. Bound GIV was visualized by immunoblotting using anti-GIV-CT rabbit polyclonal Ab. Equal loading of GST proteins was confirmed by Ponceau S staining.

(B) Comparison of yeast Exo70p [PDB: 2B7M; (Hamburger et al., 2006)] and mouse Exo70 [PDB: 2PFT; (Moore et al., 2007)] structures, visualized using Molsoft ICM pro.

(C) Equal aliquots of recombinant His-GIV-CT (~ 3 µg) were used in GST pulldown assays with GST, GST-Exo70p-WT and two previously defined Bem1p-binding deficient complex mutants of GST-Exo70 (mutant M26 and M30, each carrying numerous point mutations chosen based on surface exposed charged residues) (Liu and Novick, 2014). Bound GIV was visualized by immunoblotting using anti-His mAb. Equal loading of GST proteins was confirmed by Ponceau S staining.

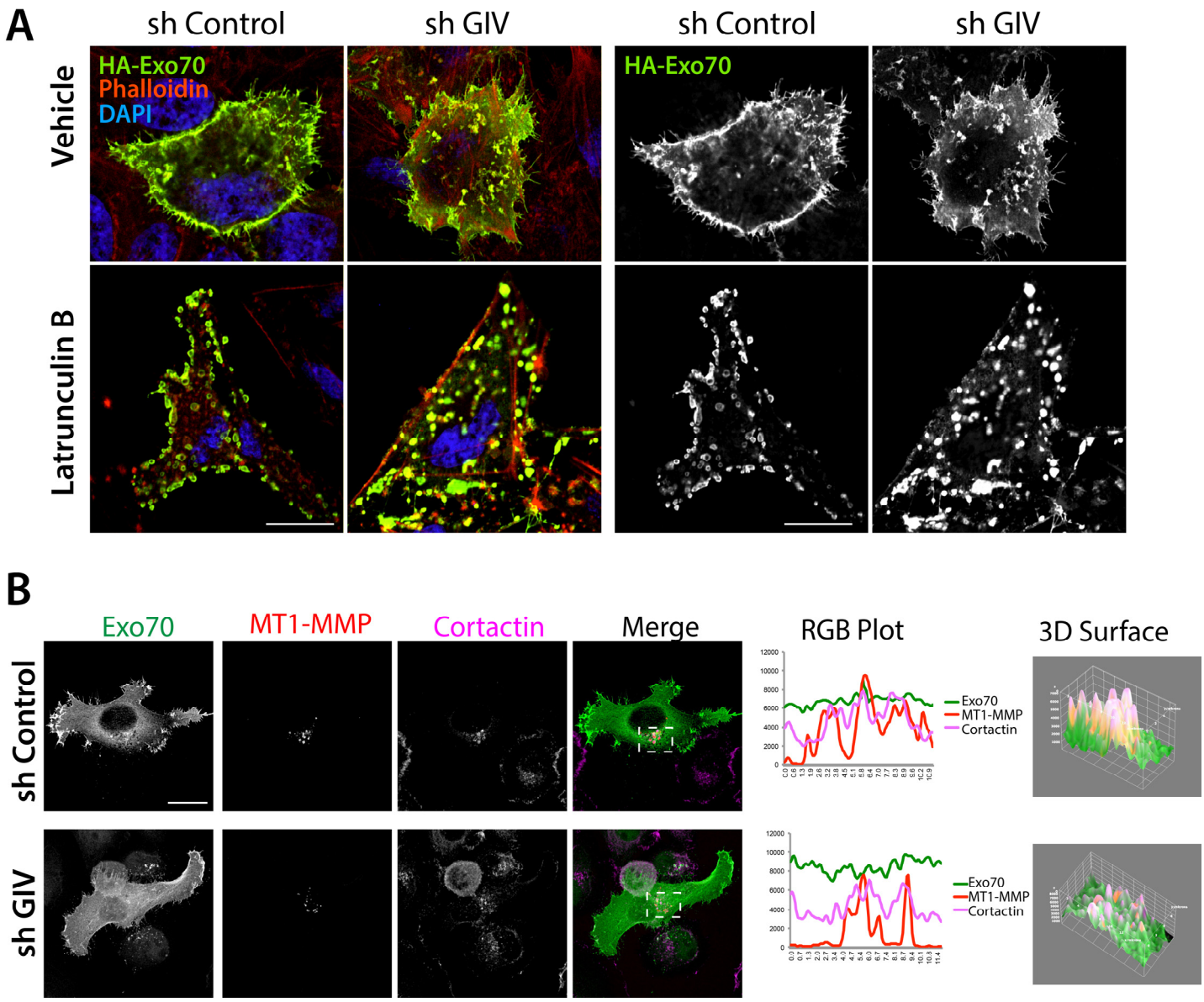

Supplementary Figure 3 [related to Figure 2]

GIV is required for the localization of Exo70 and for the delivery of trans-membrane MT1-MMP cargo to the podosomes.

(A) Control (sh Control) or GIV-depleted (sh GIV) MDA-MB-231 cells exogenously expressing HA-Exo70 were treated (lower panel) or not (vehicle) with a drug that depolymerizes actin cytoskeleton, Latrunculin B (25 μM, 24 h) prior to fixation with PFA. Fixed cells were stained for HA (green, Exo70), Phalloidin (red; actin) and DAPI (blue, nuclei) and analyzed by confocal microscopy. Representative deconvolved images are shown. Scale bar = 10 μm.

(B) Control (sh Control) or GIV-depleted (sh GIV) MDA-MB-231 cells exogenously co-expressing HA-Exo70 and MT1-MMP-mCherry plated on gelatin were fixed and stained for cortactin (a marker of cellular podosome). Representative deconvolved images are shown. Scale bar = 10 μm. Insets were analyzed by rendering 3D surface plots and line scans were taken to generate RGB plots using ImageJ.

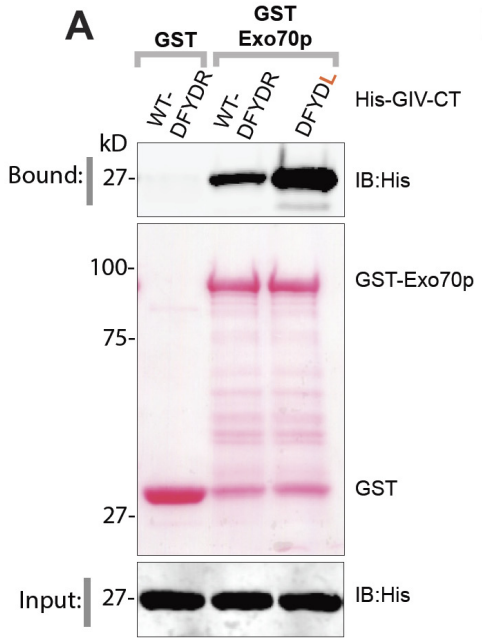

B

GIV Mutants Tested	Binding to Exo70
PGDAYDR^{1745}	----
PADFYDR^{1745}	-
AADFYDR^{1745}	-
AADAYDR^{1745}	----
PGRFYDR^{1745}	----
PGDFYRR^{1745}	+
PGAFYDR^{1745}	-
PGDFYAR^{1745}	----
PGDFADR^{1745}	--
PGAFYAR^{1745}	--
PGDFYDL^{1745}	+++

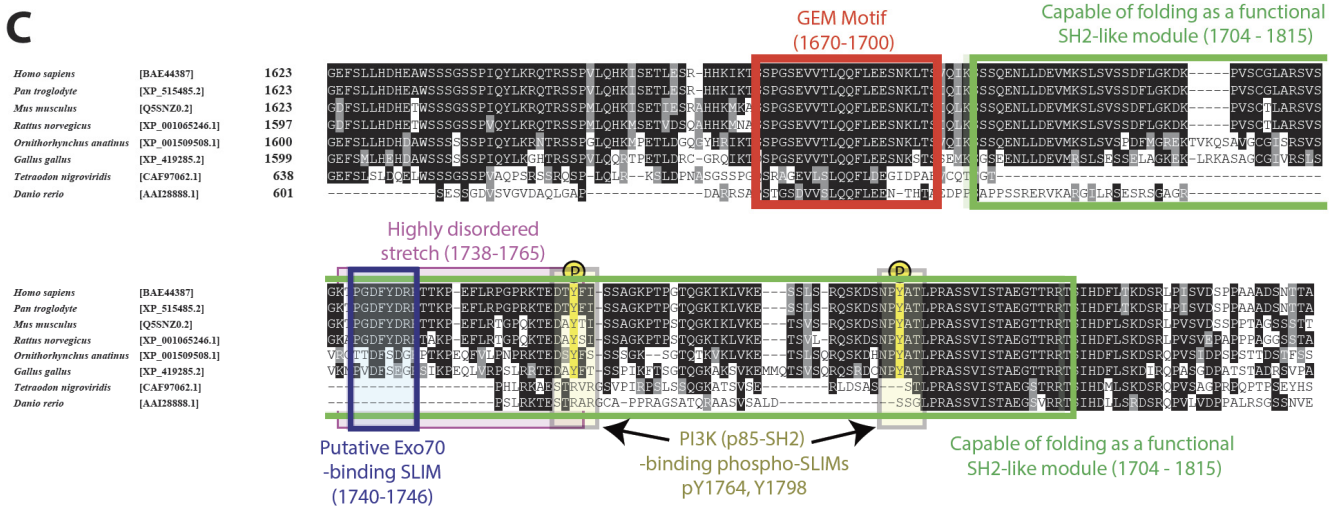

Supplementary Figure 4 (related to Fig 3)

A short linear motif within the disordered C-terminus of GIV mediates binding to Exo70.

(A) Equal aliquots of WT (^{1741}DFYDR^{1745}) or mutant (^{1741}DFYD**R**»**L**^{1745}) recombinant His-GIV-CT (~ 3 µg) were used in GST pulldown assays with GST and GST-Exo70p. Bound GIV was visualized by immunoblotting using anti-His mAb. Binding of the ^{1741}DFYD**R**»**L**^{1745} mutant GIV was consistently seen to be increased ~2-3 fold. Equal loading of GST proteins was confirmed by Ponceau S staining.

(B) Table summarizing the impact of various GIV mutations within and flanking the short linear motif ^{1739}PGDFYDR^{1745} on Exo70 binding, as assessed during *in vitro* GST pulldown assays (see **Fig 3**).

(C) Sequence alignment of GIV's C-terminus displaying a complete catalog of previously validated short linear motifs (SLIMS) and modules; the position of the newly identified Exo70-binding SLIM (aa 1740-1746) is shown in black. Because this SLIM is located within a highly disordered stretch (pink; aa 1738-1765; identified using InterPro [https://www.ebi.ac.uk/interpro/] and confirmed using MobiDB [http://mobidb.bio.unipd.it/]), it is likely to be impacted by conformational plasticity. Because multiple phosphosites flank this SLIM, it is likely that binding of GIV to Exo70 is regulated by post-translational modifications.

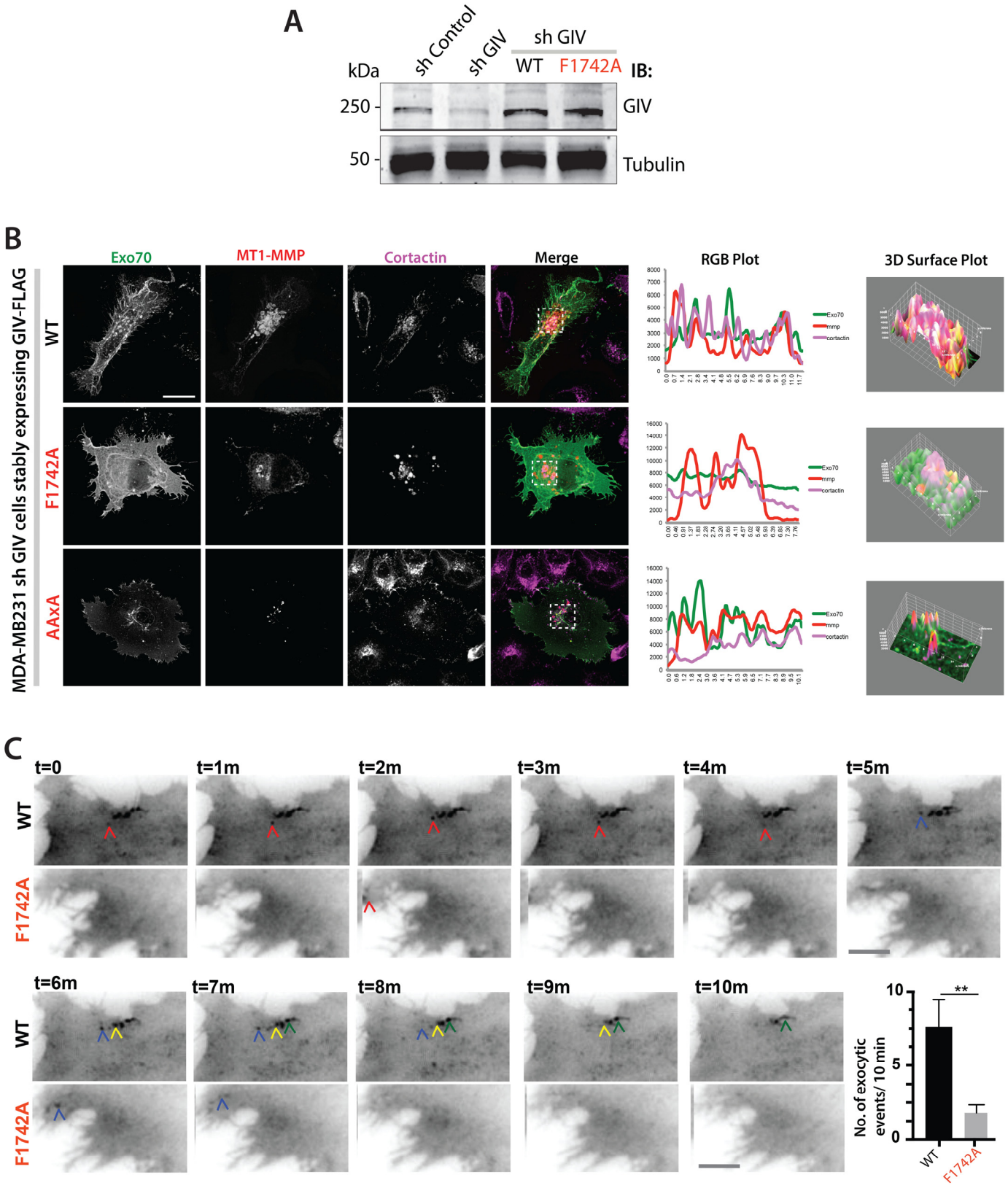

Supplementary Figure 5 (related to Fig 4)

The Exo70•GIV interaction is required for the exocytic delivery of MT1-MMP to cellular podosomes.

(A) Immunoblots of lysates of control (sh Control) and GIV-depleted (sh GIV) MDA MB231 cells stably expressing GIV-FLAG WT and Exo70-binding deficient F1742A mutant constructs.

(B) GIV-depleted (sh GIV) MDA-MB-231 cells stably expressing WT or mutant full length GIV proteins were transfected with HA-Exo70 (green) and MT1-MMP-mCherry (red) were fixed and stained for cortactin (a marker of cellular podosome). Representative deconvolved images are shown. Scale bar = 10 μm. Insets were analyzed by rendering 3D surface plots and line scans were taken to generate RGB plots using ImageJ.

(C) GIV-depleted (sh GIV) MDA-MB-231 cells stably expressing WT or mutant full length GIV proteins were transfected with MT1-MMP-pHLuorin were plated on a layer of unlabeled gelatin and imaged by TIRF microscopy. *Left:* Still frames from a 10 min long movie (Supplementary movies 3, 5). Scale bar = 2.5 μm. *Bottom right:* Bar graph shows the number of exocytic events that were encountered during the 10-min long span. Each colored arrowhead tracks one vesicle. N = ~ 5-10 cells/assay. Data are represented as mean +/- S.E.M. *p* values, **0.01.

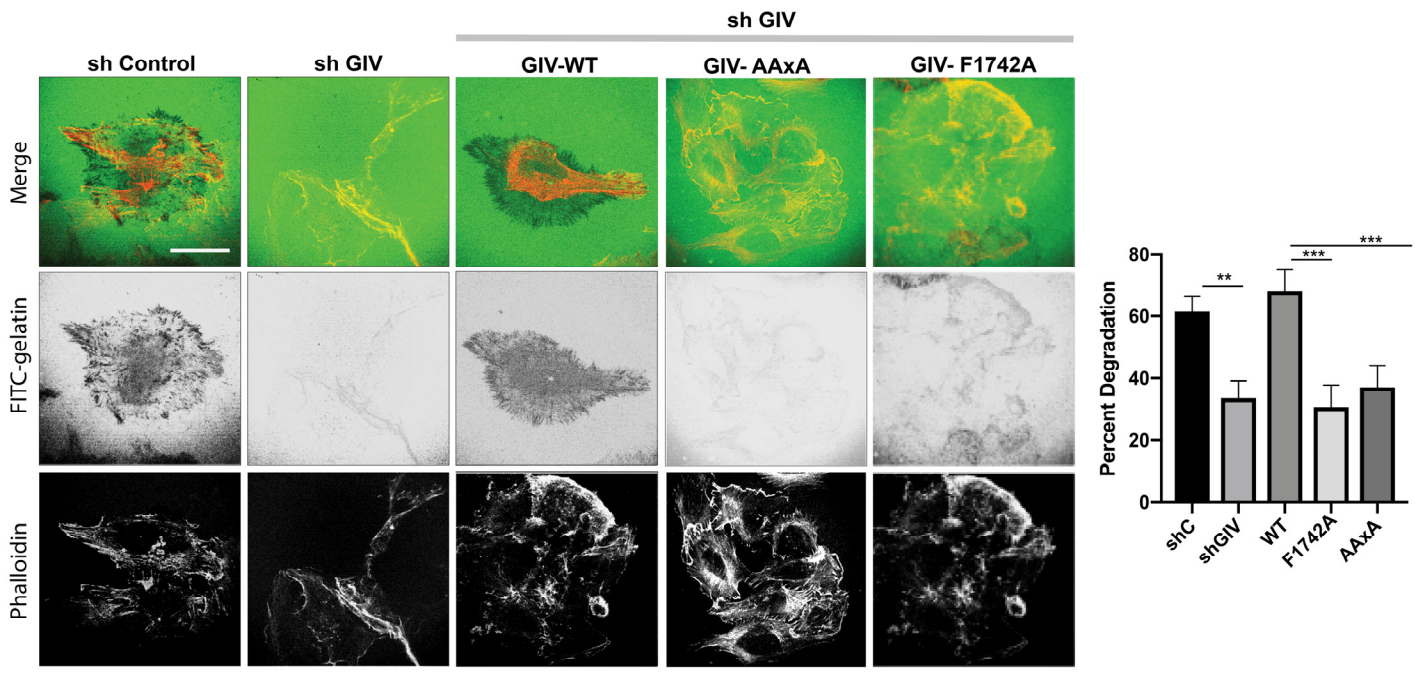

Supplementary Figure 6 (related to Fig 4)

The Exo70•GIV interaction is required for the degradation of extracellular matrix at focal adhesions.

Left: Control (sh Control), GIV-depleted (sh GIV) MDA-MB-231 cells and GIV-depleted cells stably expressing full length WT or Exo70-binding deficient mutant GIV proteins were plated for 5 h on FITC-conjugated cross-linked gelatin (green), and then fixed and stained for F-actin (Phalloidin; red). Representative images are shown. Scale bar = 15 μm.

Right: Bar graphs display the % of cells that showed degradation of gelatin. N = ~100-200 cells /experiment x 3. Data are represented as mean +/- S.E.M. *p* values, * 0.05; **0.01; ***0.001.

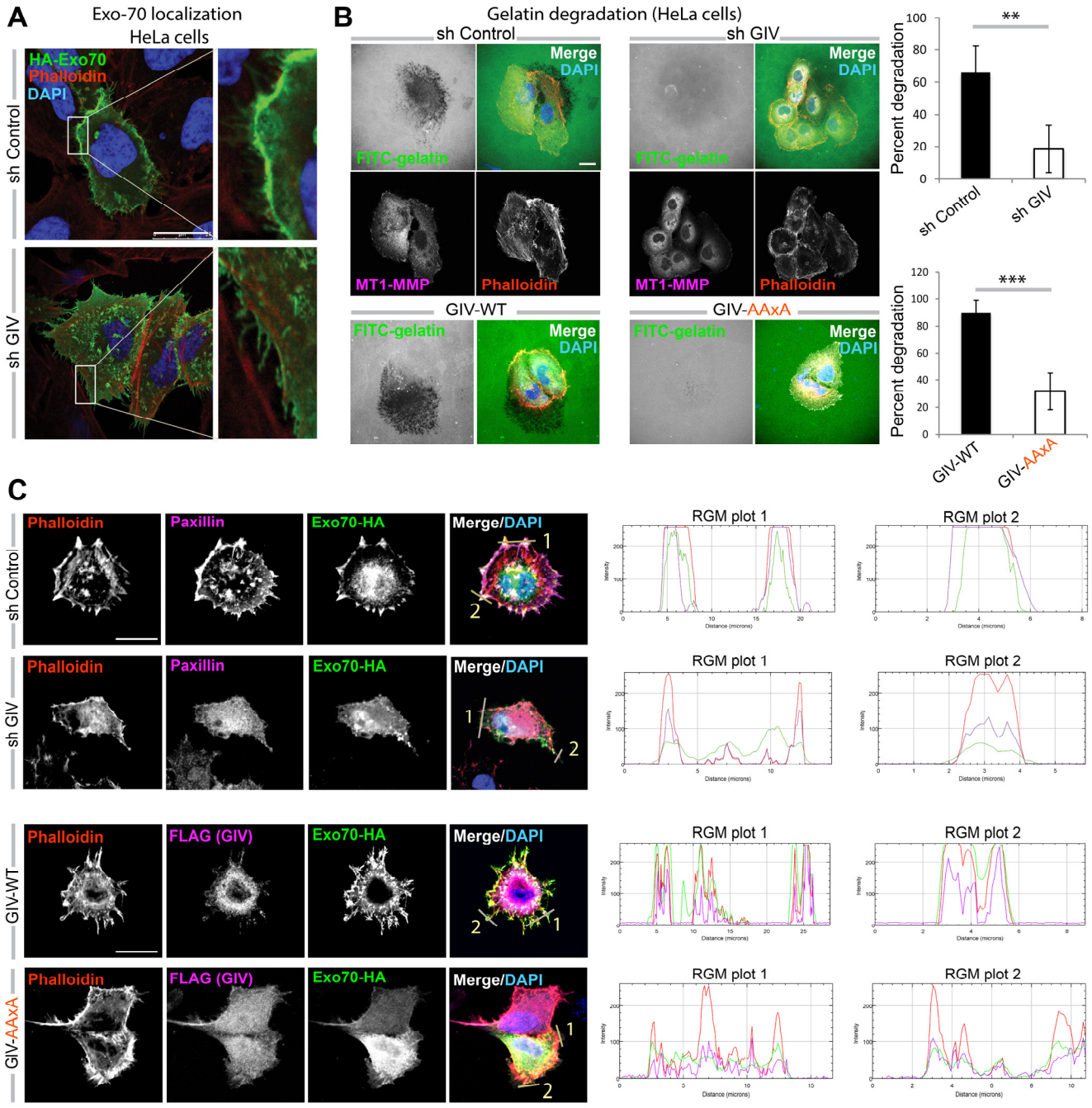

Supplementary Figure 7 (related to Fig 4)

Key findings in MDA-MB231 breast cancer cells were reproduced also in HeLa cervical cancer cells.

(A) Control (sh Control), GIV-depleted (sh GIV) HeLa cells and GIV-depleted cells expressing HA-Exo70 were fixed and stained for HA (green, Exo70), Phalloidin (red; actin) and DAPI (blue, nuclei) and analyzed by confocal microscopy. Representative deconvolved images are shown. Insets on the right show magnified fields within boxes on the left. Scale bar = 10 μm.

(B) *Left*: Control (sh Control), GIV-depleted (sh GIV) HeLa cells (top) and GIV-depleted cells expressing wither the full length GIV-WT or the Exo70-binding deficient mutant GIV (AAxA) proteins were plated for 5 h on FITC-conjugated cross-linked gelatin (green), and then fixed and stained for F-actin (Phalloidin; red).

Representative images are shown. ***Right***: Bar graphs display the % of cells that showed degradation of gelatin. N = ~100-200 cells /experiment x 3. Data are represented as mean +/- S.E.M. *p* values, * 0.05; **0.01; ***0.001. Scale bar = 10 μm.

(C) Cells in B stably expressing WT or AAxA mutant full length GIV proteins were transfected with HA-Exo70, fixed and stained for Exo-70 (HA) and either paxillin (a marker of focal adhesions; top) or GIV (FLAG). Representative deconvolved images are shown. Scale bar = 10 μm. Two different areas on the cell periphery (labeled 1 and 2) were analyzed for protein colocalization by generating red-green-magenta (RGM) plots using ImageJ.

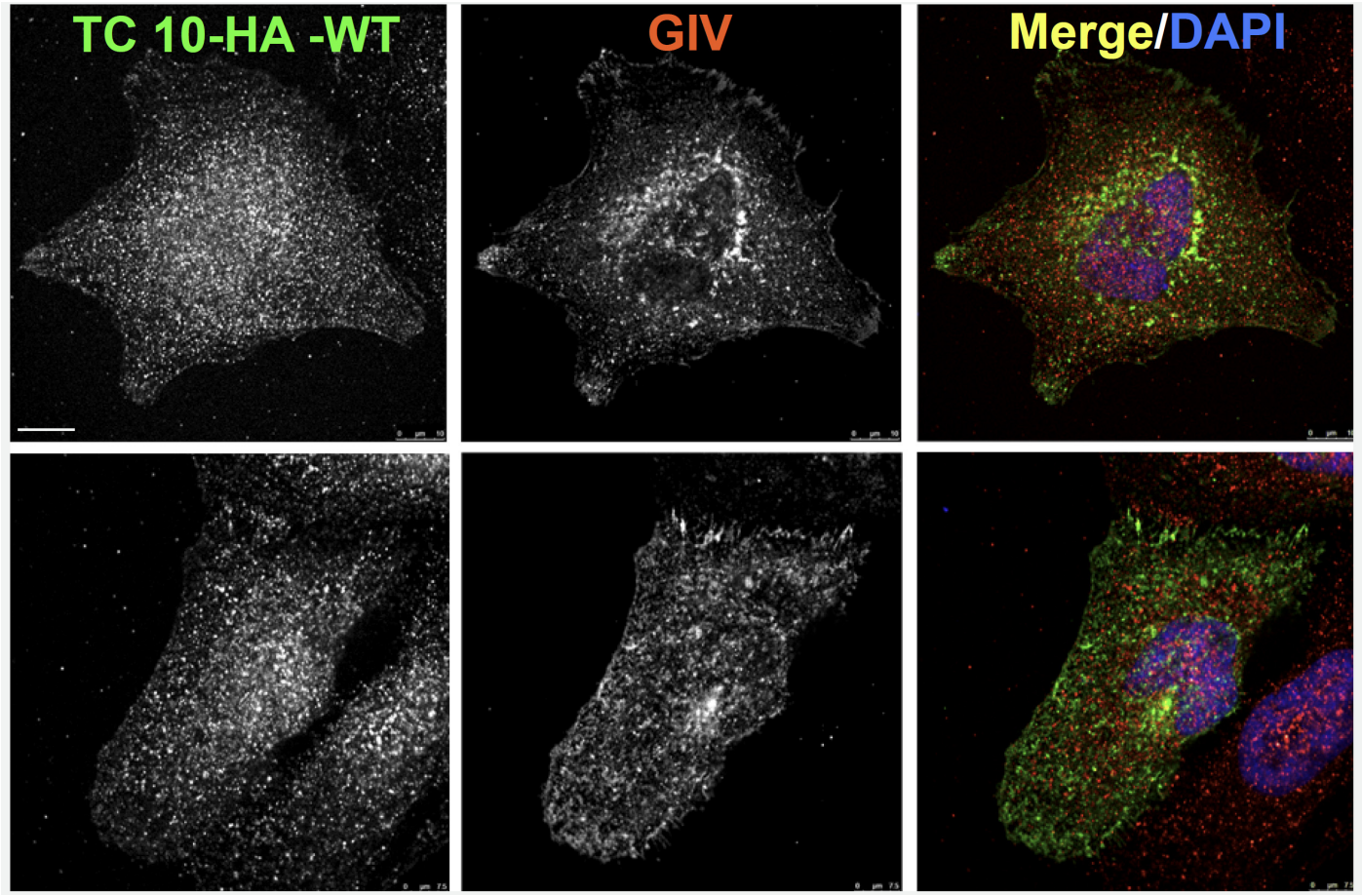

Supplementary Figure 8 (related to Fig 6)

TC10-WT cannot recruit endogenous GIV to the PM sites.

MDA MB231 cells exogenously expressing TC10-WT-HA (green) were fixed and stained for endogenous GIV (red). Representative images of transfected cells are shown. Red and green panels are shown in grey scale. Scale bar = 10 μm.

REFERENCES CITED

AZNAR, N., PATEL, A., ROHENA, C. C., DUNKEL, Y., JOOSEN, L. P., TAUPIN, V., KUFAREVA, I., FARQUHAR, M. G. & GHOSH, P. 2016. AMP-activated protein kinase fortifies epithelial tight junctions during energetic stress via its effector GIV/Girdin. *Elife,* 5.

BOS, P. D., ZHANG, X. H., NADAL, C., SHU, W., GOMIS, R. R., NGUYEN, D. X., MINN, A. J., VAN DE VIJVER, M. J., GERALD, W. L., FOEKENS, J. A. & MASSAGUE, J. 2009. Genes that mediate breast cancer metastasis to the brain. *Nature,* 459**,** 1005-9.

COX, D. R. 1972. Regression models and life tables (with discussion). *J R Statist Soc,* B**,** 187-220.

GARCIA-MARCOS, M., GHOSH, P. & FARQUHAR, M. G. 2009. GIV is a nonreceptor GEF for G alpha i with a unique motif that regulates Akt signaling. *Proc Natl Acad Sci U S A,* 106**,** 3178-83.

GARCIA-MARCOS, M., KIETRSUNTHORN, P. S., PAVLOVA, Y., ADIA, M. A., GHOSH, P. & FARQUHAR, M. G. 2012. Functional characterization of the guanine nucleotide exchange factor (GEF) motif of GIV protein reveals a threshold effect in signaling. *Proc Natl Acad Sci U S A,* 109**,** 1961-6.

GHOSH, P., GARCIA-MARCOS, M., BORNHEIMER, S. J. & FARQUHAR, M. G. 2008. Activation of Galphai3 triggers cell migration via regulation of GIV. *J Cell Biol,* 182**,** 381-93.

HAMBURGER, Z. A., HAMBURGER, A. E., WEST, A. P., JR. & WEIS, W. I. 2006. Crystal structure of the S.cerevisiae exocyst component Exo70p. *J Mol Biol,* 356**,** 9-21.

HORZUM, U., OZDIL, B. & PESEN-OKVUR, D. 2014. Step-by-step quantitative analysis of focal adhesions. *MethodsX,* 1**,** 56-9.

KAPLAN EL, M. P. 1958. Nonparametric estimation from incomplete observations. *J Am Stat Assoc,* 53**,** 457-481.

LIN, C., EAR, J., PAVLOVA, Y., MITTAL, Y., KUFAREVA, I., GHASSEMIAN, M., ABAGYAN, R., GARCIA-MARCOS, M. & GHOSH, P. 2011. Tyrosine phosphorylation of the Galpha-interacting protein GIV promotes activation of phosphoinositide 3-kinase during cell migration. *Sci Signal,* 4**,** ra64.

LIN, W. H., ASMANN, Y. W. & ANASTASIADIS, P. Z. 2015. Expression of polarity genes in human cancer. *Cancer Inform,* 14**,** 15-28.

LIU, D. & NOVICK, P. 2014. Bem1p contributes to secretory pathway polarization through a direct interaction with Exo70p. *J Cell Biol,* 207**,** 59-72.

LOPEZ-SANCHEZ, I., MA, G. S., PEDRAM, S., KALOGRIOPOULOS, N. & GHOSH, P. 2015. GIV/girdin binds exocyst subunit-Exo70 and regulates exocytosis of GLUT4 storage vesicles. *Biochem Biophys Res Commun,* 468**,** 287-93.

MIDDE, K., SUN, N., ROHENA, C., JOOSEN, L., DHILLON, H. & GHOSH, P. 2018. Single-Cell Imaging of Metastatic Potential of Cancer Cells. *iScience,* 10**,** 53-65.

MINN, A. J., GUPTA, G. P., SIEGEL, P. M., BOS, P. D., SHU, W., GIRI, D. D., VIALE, A., OLSHEN, A. B., GERALD, W. L. & MASSAGUE, J. 2005. Genes that mediate breast cancer metastasis to lung. *Nature,* 436**,** 518-24.

MOORE, B. A., ROBINSON, H. H. & XU, Z. 2007. The crystal structure of mouse Exo70 reveals unique features of the mammalian exocyst. *J Mol Biol,* 371**,** 410-21.

PETO, R., PIKE, M. C., ARMITAGE, P., BRESLOW, N. E., COX, D. R., HOWARD, S. V., MANTEL, N., MCPHERSON, K., PETO, J. & SMITH, P. G. 1977. Design and analysis of randomized clinical trials requiring prolonged observation of each patient. II. analysis and examples. *Br J Cancer,* 35**,** 1-39.

SAHOO, D., DILL, D. L., TIBSHIRANI, R. & PLEVRITIS, S. K. 2007. Extracting binary signals from microarray time-course data. *Nucleic Acids Res,* 35**,** 3705-12.

SAKURAI-YAGETA, M., RECCHI, C., LE DEZ, G., SIBARITA, J. B., DAVIET, L., CAMONIS, J., D'SOUZA-SCHOREY, C. & CHAVRIER, P. 2008. The interaction of IQGAP1 with the exocyst complex is required for tumor cell invasion downstream of Cdc42 and RhoA. *J Cell Biol,* 181**,** 985-98.

WANG, Y., KLIJN, J. G., ZHANG, Y., SIEUWERTS, A. M., LOOK, M. P., YANG, F., TALANTOV, D., TIMMERMANS, M., MEIJER-VAN GELDER, M. E., YU, J., JATKOE, T., BERNS, E. M., ATKINS, D. & FOEKENS, J. A. 2005. Gene-expression profiles to predict distant metastasis of lymph-node-negative primary breast cancer. *Lancet,* 365**,** 671-9.

XIONG, X., XU, Q., HUANG, Y., SINGH, R. D., ANDERSON, R., LEOF, E., HU, J. & LING, K. 2012. An association between type Igamma PI4P 5-kinase and Exo70 directs E-cadherin clustering and epithelial polarization. *Mol Biol Cell,* 23**,** 87-98.